

**AN EXPERIMENTAL STUDY OF THE COANDA AIR JET AND
ITS APPLICATION TO WEB SUPPORT AND TRACTION**

By

VIJAY RAGHAVAN ARAVAMUDHAN

Bachelor of Engineering

University of Madras

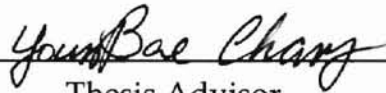
Madras, India

1996

Submitted to the Faculty of the
Graduate College of the
Oklahoma State University
in partial fulfillment of
the requirements for
the Degree of
MASTER OF SCIENCE
May, 1998

AN EXPERIMENTAL STUDY OF THE COANDA AIR JET AND
ITS APPLICATION TO WEB SUPPORT AND TRACTION

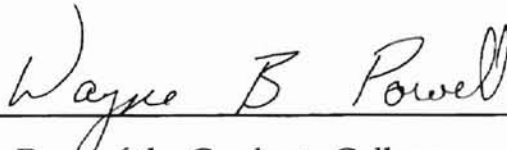
Thesis Approved:



Thesis Advisor







Dean of the Graduate College

ACKNOWLEDGMENTS

I wish to express my sincere appreciation and gratitude to Dr. Young Bae Chang for his intelligent supervision, patience and enthusiasm he showed during the course of this research work and during my career at Oklahoma State University. I am also indebted to Dr. Peter M. Moretti for his suggestions and guidance throughout the course of this research. I would also like to thank Dr. Richard L. Lowery for his suggestions and help.

I am greatly indebted to my parents Mr. S. Aravamudhan and Mrs. K. Mythili and my sister Ms. Krishna for their prayers and all the moral support they provided me during my undergraduate as well as graduate study (when I was with them and also when I was away from them). I would like to express my deepest gratitude to my cousins Srikanth, Sujatha, Venkat, Partha and Vathsan for giving me moral support when I was away from home.

Moreover, I wish to express my sincere thanks to all those connected with the Web Handling Research Center and the School of Mechanical and Aerospace Engineering at Oklahoma State University who provided suggestions and help to make this research work a great success. I would like to especially thank Mr. Jerry Dale for his invaluable help in machining the necessary parts for the test setup.

I would also like to thank my friends, Aniruddha, Bommu, Anuj, Murali, Kannan, Thirumal and Satheesh for giving me great company which made my life at Oklahoma State University a pleasantly memorable one.

I would like to express my sincere thanks to Oklahoma State University's Web Handling Research Center for providing financial support during the course of this research.

Vijay Raghavan Aravamudhan

TABLE OF CONTENTS

	Page
CHAPTER 1: INTRODUCTION	1
1.1 BACKGROUND	1
1.2 PROBLEM STATEMENT	2
1.3 OBJECTIVES AND SCOPE OF STUDY	2
CHAPTER 2: LITERATURE REVIEW	4
CHAPTER 3: EXPERIMENTAL SETUP AND PROCEDURE	10
3.1 COANDA AIR JET IN FREE SPACE	10
3.1.1 <i>Experimental setup</i>	<i>10</i>
3.1.2 <i>Procedure for testing the Coanda air jet in free space</i>	<i>14</i>
3.2 INTERACTION OF THE COANDA AIR JET WITH A RIGID WEB	16
3.2.1 <i>Experimental setup</i>	<i>16</i>
3.2.2 <i>Procedure for testing the interaction of the Coanda air jet with a rigid web</i>	<i>23</i>
CHAPTER 4: RESULTS AND DISCUSSION	26
4.1 BEHAVIOR OF THE COANDA AIR JET IN FREE SPACE	26
4.1.1 <i>Effects of nozzle width</i>	<i>31</i>
4.1.2 <i>Effects of nozzle offset</i>	<i>34</i>
4.1.3 <i>Effects of radius of curvature</i>	<i>36</i>
4.2 INTERACTION OF THE COANDA AIR JET WITH A RIGID, STATIONARY WEB	38
4.2.1 <i>Effects of supply air pressure</i>	<i>42</i>
4.2.1.1 <i>Pressure profiles</i>	<i>42</i>
4.2.1.2 <i>Aerodynamic friction drag</i>	<i>44</i>
4.2.2 <i>Effects of flotation height of the web</i>	<i>47</i>
4.2.2.1 <i>Pressure profiles</i>	<i>47</i>
4.2.2.2 <i>Aerodynamic friction drag</i>	<i>49</i>
4.2.3 <i>Effects of nozzle width</i>	<i>51</i>
4.2.3.1 <i>Pressure profiles</i>	<i>51</i>
4.2.3.2 <i>Aerodynamic friction drag</i>	<i>52</i>
4.3 DISCUSSION AND COMPARISON WITH OTHER'S STUDY	54
4.4 UNCERTAINTY OF THE EXPERIMENTAL DATA	58
CHAPTER 5: ANALYSIS OF EXPERIMENTAL DATA	61
5.1 DIMENSIONAL ANALYSIS	61
5.2 DIMENSIONAL ANALYSIS FOR THE COANDA JET	63
CHAPTER 6: CONCLUSIONS	68
CHAPTER 7: RECOMMENDATIONS FOR FUTURE STUDY	70
REFERENCES	72
APPENDIX: PROGRAMMING ON LABVIEW FOR THE COANDA JET EXPERIMENT	74

LIST OF FIGURES

Figure 3.1: Schematic of the experimental setup for the Coanda air jet in free space	13
Figure 3.2: Schematic of the pressure taps on the rigid web.....	18
Figure 3.3: Schematic of the setup for the interaction of the Coanda air jet with a rigid, stationary web.....	21
Figure 3.4: Picture (side view) of the setup for the interaction of the Coanda air jet with a rigid, stationary web	21
Figure 3.5: Picture (front view) of the setup for the interaction of the Coanda air jet with a rigid, stationary web	22
Figure 4.1: Effect of supply air pressure for the Coanda air jet in free space ($R = 0.078$ in, $b = 0.01$ in).....	28
Figure 4.2: Effect of air pressure for the Coanda air jet in free space ($R = 0.078$ in, $b = 0.02$ in).....	30
Figure 4.3: Effect of air pressure for the Coanda air jet in free space ($R = 0.141$ in, $b = 0.04$ in).....	30
Figure 4.4: Effect of nozzle width for the Coanda air jet in free space ($R = 0.078$ in).....	31
Figure 4.5: Effect of nozzle width for the Coanda air jet in free space ($R = 0.078$ in) after manipulations.....	33
Figure 4.6: Effect of nozzle height for the Coanda air jet in free space ($R = 0.078$ in).....	34
Figure 4.7: Effect of nozzle height for the Coanda air jet in free space ($R = 0.141$ in).....	35
Figure 4.8: Effect of radius of curvature for the Coanda air jet in free space ($h = 0.000$ in).....	37
Figure 4.9: Pressure profile on the rigid web ($R = 0.172$ in, $b = 0.030$ in, $h = 0.000$ in, $h_1 = 0.150$ in, $P = 12$ in H_2O)	39
Figure 4.10: Friction drag on the rigid web ($R = 0.172$ in, $b = 0.030$ in, $h = 0.000$ in, $h_1 = 0.150$ in, $P = 12$ in H_2O).....	41
Figure 4.11: Effect of supply air pressure on pressure profile ($R = 0.172$ in, $b = 0.035$ in, $h = 0.000$ in, $h_1 = 0.150$ in, $h_1/b = 4.29$)	42
Figure 4.12: Effect of supply air pressure on pressure profile ($R = 0.172$ in, $b = 0.025$ in, $h = 0.000$ in, $h_1 = 0.180$ in, $h_1/b = 7.20$)	43
Figure 4.13: Effect of supply air pressure on pressure profile ($R = 0.172$ in, $b = 0.040$ in, $h = 0.000$ in, $h_1 = 0.180$ in, $h_1/b = 4.50$)	44
Figure 4.14: Effect of supply air pressure on friction drag ($R = 0.172$ in, $b = 0.035$ in, $h = 0.000$ in, $h_1 = 0.180$ in, $h_1/b = 5.14$)	45
Figure 4.15: Effect of supply air pressure on friction drag ($R = 0.172$ in, $b = 0.025$ in, $h = 0.000$ in, $h_1 = 0.180$ in, $h_1/b = 7.20$)	46
Figure 4.16: Effect of supply air pressure on friction drag ($R = 0.172$ in, $b = 0.040$ in, $h = 0.000$ in, $h_1 = 0.180$ in, $h_1/b = 4.50$)	46

Figure 4.17: Effect of flotation height on pressure profile ($R = 0.172$ in, $b = 0.025$ in, $h = 0.000$ in, $P = 12$ in H_2O)	47
Figure 4.18: Effect of flotation height on pressure profile ($R = 0.172$ in, $b = 0.035$ in, $h = 0.000$ in, $P = 16$ in H_2O)	48
Figure 4.19: Effect of flotation height on friction drag ($R = 0.172$ in, $b = 0.030$ in, $h = 0.000$ in).....	49
Figure 4.20: Effect of flotation height on friction drag ($R = 0.172$ in, $b = 0.035$ in, $h = 0.000$ in).....	50
Figure 4.21: Effect of nozzle width on pressure profile ($R = 0.172$ in, $h = 0.000$ in, $P = 8$ in H_2O , $h_1 = 0.120$ in).....	51
Figure 4.22: Effect of nozzle width on pressure profile ($R = 0.172$ in, $h = 0.000$ in, $P = 12$ in H_2O , $h_1 = 0.120$ in).....	52
Figure 4.23: Effect of nozzle width on friction drag ($R = 0.172$ in, $h = 0.000$ in, $h_1 = 0.120$ in).....	53
Figure 4.24: Effect of supply air pressure on friction drag ($R = 0.172$ in, $h = 0.000$ in, $h_1 = 0.150$ in).....	53
Figure 4.25: Comparison of current experiments with computational results by Thirumal (1998) for the Coanda air jet in free space (Effect of b for $R = 0.141$ in).....	54
Figure 4.26: Comparison of current experiments with computational results by Thirumal (1998) for the Coanda air jet in free space (Effect of h for $R = 0.141$ in).....	55
Figure 4.27: Comparison of current experiments with computational results by Thirumal (1998) for the interaction of the Coanda air jet with a rigid web ($R = 0.172$ in, $b = 0.025$ in, $h = 0.000$ in, $h_1 = 0.150$ in, $P = 8$ in H_2O , $h_1/b = 6.00$).....	56
Figure 4.28: Comparison of current experiments with computational results by Thirumal (1998) for the interaction of the Coanda air jet with a rigid web ($R = 0.172$ in, $b = 0.025$ in, $h = 0.000$ in, $h_1 = 0.150$ in, $P = 12$ in H_2O , $h_1/b = 6.00$).....	57
Figure 4.29: Comparison of current experiments and computational results by Thirumal (1998) for the interaction of the Coanda air jet with a rigid web ($R = 0.172$ in, $b = 0.025$ in, $h = 0.000$ in, $h_1 = 0.150$ in, $P = 8$ & 12 in H_2O , $h_1/b = 6.00$).....	58
Figure A.1: The Front Panel of the program code for testing the Coanda effect on a rigid web	75
Figure A.2: The Diagram Window of the program code for testing the Coanda effect on a rigid web	76

LIST OF TABLES

Table 4.1: Cases considered for the Coanda air jet in free space	27
Table 4.2: Cases considered for the interaction of the Coanda air jet with a rigid, stationary web ...	38
Table 5.1: Parameters affecting the behavior of the air jet and their dimensions	63
Table 5.2: Matrix of coefficients for the Π group	64
Table 5.3: Non-dimensional numbers formed using the specified parameters	67
Table A.1: Connections given for the devices in the AD Converter	74

NOMENCLATURE

b	Nozzle width
h	Nozzle offset (Height difference between the nozzle and the starting point of curvature on the vertical side of the curved surface block)
h_1	Flotation height (Distance between the rigid web and the top of the follow-up surface)
P	Supply pressure of air
R	Radius of curvature of the 90° convex surface
x	Horizontal distance from the nozzle

Note: Definition of above variables is also shown in Fig. 3.1 .

CHAPTER 1

INTRODUCTION

1.1 Background

Thin, flexible materials which are usually wound in large, cylindrical bales are known as webs. Web handling refers to the methods and operations performed to handle the webs while they are being processed. Web handling methods can be classified into two categories as contact and non-contact handling. Contact methods of web handling use rollers and other such devices to handle the webs; non-contact web handling methods use air cushions to support the web and so the web does not come into contact with any solid surface when it is being handled. Once the web is coated or printed, the web needs to be dried without causing any defects to the product. This necessitates the use of air jets for web support, transport, and control.

In general, to increase the productivity, the only avenue open is to increase the flow velocity of the web. This limitation is due to the very high expenses that would be incurred if any other method were chosen, for achieving the same boost in productivity. The flow velocity also has an upper limiting value, which is governed by the air flotation ovens through which the web passes while it is being dried. If the flow velocity is increased, the time the web stays inside air floatation ovens (used for drying the web) is reduced. This has to be compensated for either by increasing the temperature of the oven, or by increasing the size of the oven, the latter again entailing a huge investment.

1.2 Problem Statement

One of the main phenomena used by most of the air flotation devices is the Coanda effect. The Coanda air jets used inside the ovens use hot air for simultaneously drying the web. In order to improve the design of such air devices, the behavior of the Coanda air jets should be thoroughly analyzed and studied.

An extensive literature review reveals that very little work has been done that is directly related to the use of the Coanda effect for web handling. The Coanda effect has been studied by a lot of researchers mostly in relevance to the aerospace industry. The few studies related to the use of the Coanda air jet as air flotation devices, deal mainly with discrete objects and not thin webs. Due to the growing necessity for non-contact web handling techniques, a study of the Coanda effect specifically relating to its application in this area is essential. This study could reveal the physics behind many problems that occur during web handling.

1.3 Objectives and Scope of Study

The primary objectives of this study are as follows:

1. Study the behavior of the Coanda jet without the physical existence of a web

2. Use the experimental data to obtain the functional relationship(s) between the non-dimensional numbers so as to optimize the geometry of the Coanda nozzle
3. Study the interaction of the Coanda air jet with a rigid, stationary web placed above the nozzle region so as to evaluate the possibility of using the Coanda air jet for web support, transport and lateral control

CHAPTER 2

LITERATURE REVIEW

The Coanda effect is named after the person who discovered it, Henry Coanda. As most discoveries go, this phenomenon was discovered accidentally by Coanda when he was testing a new plane with two primitive jet engines designed by himself. The burned gasses and the flames were being drawn toward (instead of away from) the wooden fuselage, thus causing the plane to crash. Coanda studied this new phenomenon which was later named as the Coanda effect by von Karman (Reba, 1996).

The physics of reattachment of an air jet, after a brief separation, are clearly explained by Squire (1950). He explains that after leaving the nozzle, the air jet is under the influence of the highly unstable shear layers on both sides which cause the reattachment of the air jet to the solid wall.

The air jet exiting the exhaust from a Vertical Take-Off and Landing (VTOL) aircraft was studied by Glauert (1956). This exhaust air jet upon striking the ground, spreads out radially. He used a similarity approach to solve the boundary layer equations for a radial wall jet with two similarity exponents giving the variation with distance of the maximum velocity and the jet width.

Bakke (1958) dealt with the experimental investigation of a turbulent low speed, radial air jet moving over a flat surface. This was similar to the wall jet described and studied by Glauert (1956) but the main importance was given to the mean velocity distribution and the rate of growth of the jet.

Among the first studies concerning applications of the Coanda effect, some were made by Bourque and Newman (1960). They discussed the reattachment of a two-dimensional, incompressible air jet when it passed out of a nozzle and passed near an inclined, flat plate. They found that the length of the plate and the Reynolds number cease to affect the behavior of the air jet when they are large and then the inclination of the plate is the only other parameter influencing the flow.

Newman (1961) studied the flow of a two-dimensional incompressible, turbulent air jet flowing around a circular cylinder and a jet flowing adjacent to an inclined flat plate. For the case of the circular cylinder, he said that for large Reynolds numbers, the equation governing the flow of air can be expressed as

$$\frac{(P_{\infty} - P_s)a}{(P - P_{\infty})b} = f(\theta) \quad (2.1)$$

where P = supply air pressure

P_{∞} = surrounding air pressure

P_s = pressure on the surface of the cylinder

b = width of slot

a = radius of cylinder

θ = angle of turn of the fluid around the cylinder

In April, 1965, there was a colloquium held in Berlin which was called the First European Mechanics Colloquium on the Coanda Effect. In a report of the proceedings of this colloquium, Wille and Fernholz (1965) describe briefly almost

all the works done on the Coanda effect until then, including some interesting applications of the Coanda effect like a fluidic amplifier and an artificial respirator. One important point agreed upon by everybody in the colloquium was that the Coanda phenomenon was due to two contributory effects: the curvature forced upon the jet by the convex body and the entrainment of fluid into the jet due to turbulent mixing. Another point reported in the colloquium was that “the jet flow is likely to be detached if the height of the jet around the throat is large in relation to the radius of the cylinder.”

Two other pioneers in the field of the Coanda effect were Felsing and Moller (1969). In their paper, they introduce a new technique for controlling the axisymmetric air jets from the exhaust of VTOL aircraft by using the Coanda effect instead of direction flaps. This entailed a study of the effect of introducing a jet normal to a cylindrical surface while a main jet followed the cylinder. They found that just after the point of separation, the static surface pressure rapidly approached the static pressure of the surrounding fluid which might also provide a fast control of the thick jet VTOL aircraft.

An experimental study on the deflection and reattachment of a radial jet discharged from a cylindrical nozzle onto an adjacent disc plate in the presence of a lateral control jet was conducted by Tanaka and others (1987). They studied the flow field near the nozzle exit for various flow rates of the control jet and found that the velocity profile, shape and length of a jet potential core were dependent on the control flow rate.

The next step towards studying the Coanda effect was taken by Morrison and Gregory-Smith (1984) when they used a tulip-shaped wall structure and a convergent nozzle. Their computational study included the surface stress imposed by both the longitudinal curvature and the divergence due to the axisymmetric tulip to try to predict the development of the jet in subsonic flow. Mixing and combustion were also incorporated into their program code and the results were compared with the experimental data recorded by Morrison.

The tulip shaped curved wall structure was also utilized by Gregory-Smith and Gilchrist (1987) along with a convergent nozzle for studying supersonic flow. They noticed that the wall jet was separated from the wall and said that this separation could be approximately calculated by calculating the first shock cell structure.

One very important property of the Coanda effect is the jet's ability to have a bistable state while exiting through a nozzle and into a closed duct. This property was first studied and described by Murai and others (1989) in their paper where they describe the use of the Coanda effect to make a fluid jet (air or water) to attach itself to the opposite walls of a rectangular duct. They found that the condition for predicting the behavior of the jet was dependent on the Strouhal number and the shape factor of the channel being used.

Research conducted and published within the previous decade also included a paper by Cornelius and Lucius (1984) in which they concentrated on the parameters controlling the detachment of the Coanda jet from the curved

surface. They found that above a critical value of pressure, the air jet ceased to follow the Coanda Principle and was vectored to the surface, thus causing a jet breakaway from the surface. On the application of the Coanda effect for Circulation Control Wings, they said that due to the existence of this critical pressure, there was an upper limit on the value of the maximum lift that could be obtained using this effect.

In an abstract for their paper, Paik and others (1996) explain the behavioral patterns of the Coanda air jet as having three types of flow: a straight, non-adherent free jet, curved-surface-adherent jet, and a split, partially-adherent jet.

Marwood (1948) did an experimental study of the Coanda effect. In his report he said that the mechanism of entrainment is equally dependent on the pressure reduction in the jet and the turbulent momentum exchange in the mixing zone. He found that the reductions in the kinetic energy along the flap that he used were mainly due to the work done by the jet against increasing pressure and to the losses in the region of the separation. One important contribution of his was towards increasing the optimization of the air entrainment (for any applications that require a large volume of air flow) which he said could be achieved by increasing the overhang at the cost of a reduction in the kinetic energy of the jet. As regards an optimal design for a Coanda flap, he said that a small overhang and a small flap angle were the best choice. His work

was done using a rectangular pipe nozzle with a flat plate at the exit for providing the required deflection of the jet.

Wetmore (1972), describes in detail the method of using pneumatic techniques for transporting materials through a duct. He used materials which were spherical and cylindrical in shape and whose weights ranged from 2.5 grams to around 165 grams. His conclusions were that all the materials he used could be conveyed from one point to another using the Coanda nozzle as the pneumatic device.

Some numerical work was also done in the past few decades to theoretically predict the behavior of the jet due to the Coanda effect but these works were limited by the level of computing facilities and the knowledge of the various parameters affecting this phenomenon. In recent years, due to the tremendous improvement of hardware and software, the field of computational fluid dynamics has made great advancements. One of the most recently published papers by Sawada and Asami (1997) deals with the underexpanded Coanda jet flow in a supersonic environment using the Navier-Stokes equations in two and three dimensions. The geometry considered in this study included a circular cylindrical wall and a supersonic jet flow for which experimental data was available so that the two results could be compared.

CHAPTER 3 EXPERIMENTAL SETUP AND PROCEDURE

3.1 Coanda air jet in free space

3.1.1 Experimental setup

The experimental setup for this first phase of the experiment consisted of three basic parts: the nozzle, the curved surface which was placed just outside the nozzle exit, and the straight follow-up surface which followed the curved surface.

The first block of aluminum (A in Fig. 3.1), measuring about 8 inches (203 mm) high, 6 inches (152 mm) wide and 2 inches (51 mm) thick (4 inches at the top), formed one wall of the settling chamber (F) and the nozzle chamber (K). As shown in Fig. 3.1, the top part of the block A had a tapered protrusion with an angle of around 45° which ended in a knife edge. This part formed the nozzle through which the air exited. The block A could also be slid in the horizontal direction so as to change the nozzle width. This was done with two cylindrical guide pins (G) which were housed in another aluminum block (B). Both the guide pins measure 0.5 inches (13 mm) in diameter and 6.5 inches (165 mm) in length. The opposite wall of the settling chamber was made up of the aluminum block B mentioned before. The curved surface block (C), which is an aluminum block with one edge round-cut with the required radius of curvature, was positioned on the shoulder formed on the block B. The curved surface block was 4 inches (102 mm) in height, 6 inches (152 mm) in width and 2 inches (51 mm) in

length. This block C could be moved in the vertical direction so as to change the relative height between the nozzle exit and the curved surface following the nozzle. The curved surface block was guided using two cylindrical guiding pins (D). The guide pins also have the same dimensions as the previous set (0.5 inches in diameter and 6.5 inches in length). The bases of the blocks A and B were fixed firmly to an aluminum base plate (I), which is 7 inches (178 mm) long, 6 inches (152 mm) wide, and 0.75 inches (19 mm) thick.

The two side walls of the setup were made up of transparent plexiglass sheets which measure around 7.5 inches (190 mm) wide, 15 inches (381 mm) high and 0.5 inches (13 mm) thick. The aluminum blocks were fitted such that the plexiglass sheets extend about 3.5 inches (89 mm) above the top surfaces of the blocks. The reason why this was done was to reduce the effect of any air flowing in the cross-direction and thus maintain a two-dimensional airflow from the nozzle above the curved surface and the follow-up surface. The compressed air entered through the air inlet port (H) and entered the air inlet chamber. Since the air was compressed, it behaved like a jet and so to reduce the jet effect, it was passed through a settling chamber, which was filled with a porous material. The top wall of the settling chamber (J) was an aluminum angle fixed on one side to the block B. The angle was perforated so that the air could pass through it. This angle also held the porous material in place. All these aluminum blocks were mounted on another 0.75 inches (19 mm) thick aluminum plate which acted as the base (I).

One of the main concerns was that the dimensions of the slot nozzle and the other parameters might change during experimentation due to the air pressure in the chamber. To prevent this problem, all the blocks were fixed to the plexiglass on the two sides using screws. Due to the horizontal and vertical movements of the nozzle block and the curved surface block respectively, the screw-holes for these were made as slots with a very low tolerance. Corkboard was used at all the edges of the chambers so that the leakage of any air from the setup was minimized.

Another main parameter, which could not be changed but which we thought might affect the behavior of the air jet, was the surface roughness of the curved surface block and the follow-up surface. To minimize this effect, the top surfaces of these blocks were polished using a very high-grade emery paper and to minimize the occurrence of any scratches, these surfaces were later anodized. The surface roughness of each block was measured using a Mitutoyo SurfTest machine and found to be approximately 45 μ inches (1.1 μ m) or less.

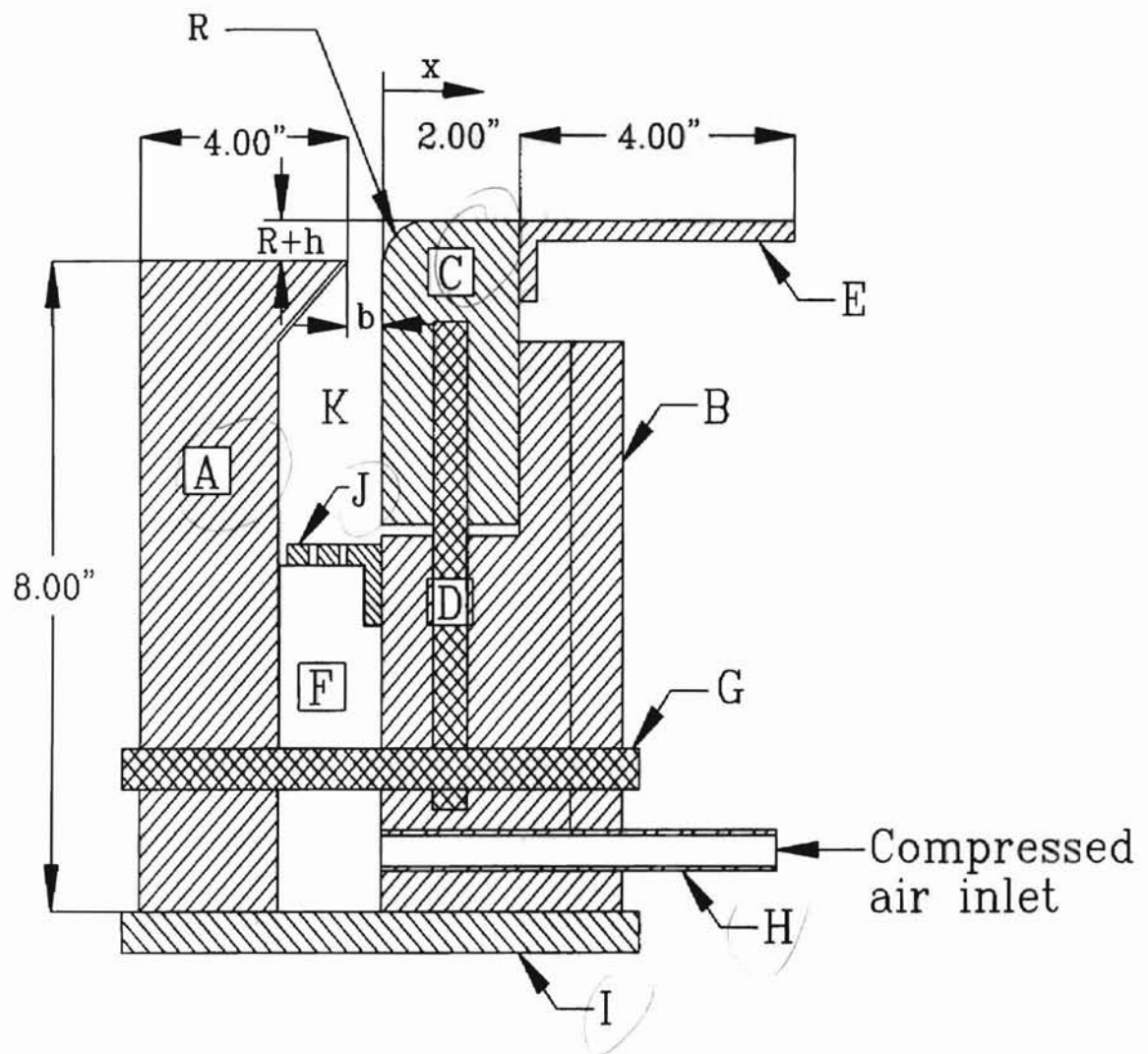


Figure 3.1: Schematic of the experimental setup for the Coanda air jet in free space

3.1.2 Procedure for testing the Coanda air jet in free space

Experiments were done with the Coanda jet in free space i.e. without any web near the nozzle. The behavior of the Coanda jet is believed to depend on various parameters such as the nozzle width, relative height between the nozzle exit and the curved surface, the roughness of the curved surface, the radius of curvature of the curved surface and the inlet pressure of the air. During the course of the experimentation, the surface roughness was kept constant while the other parameters were varied one by one.

Since varying the radius of curvature of the surface involved changing the curved surface block, this was changed the least number of times. During this first phase of the experiment, the easiest parameters that could be changed were the supply air pressure and the nozzle width. The next easiest parameter was the relative height between the nozzle exit and the top surface of the curved surface block. So the parameters were changed in the increasing order of difficulty as: (1) supply air pressure, (2) nozzle width, (3) nozzle height, and lastly (4) the radius of curvature.

Before starting any experiment, the values of all the parameters, except the supply air pressure, was fixed. All the blocks were firmly secured using the screws so that they do not slide during the course of the experiment. The nozzle width and the nozzle height were adjusted using lead screws and the values were fixed using some precision shims. Also, the vertical manometer was adjusted for zero correction before the experiment was started.

The supply air pressure was slowly increased from zero in increments of around 0.5 inches (13 mm) of water. The path of flow of the air jet out of the nozzle was felt by hand by keeping the hand at around 1 inch (25 mm) above the nozzle. One of the shortcomings of this method of measurement was that for very low supply air pressures, the human hand is not sensitive enough to sense the flow of air. So, data was not collected at such an ambiguous state. Above the threshold of sensitiveness, as the pressure was increased, it could be seen that the airflow was in the vertical direction away from the curved edge of the aluminum block. In this state, the Coanda jet was termed as being separated from the surface and so this region was named as the *Separated jet region*. The supply air pressure was slowly increased and the behavior was found to remain stable. As the air pressure crossed a certain threshold, the behavior of the jet was found to become bistable. By this we mean that the air jet either went in a vertical path away from the curved surface or followed the contour of the curved surface and went parallel to it, depending on the way it was deflected. The jet was deflected by hand. In this state, the region was named as the *Bistable region* since the jet was stable in both the types of behavior. Again the supply air pressure was slowly increased and the behavior of the jet noted. After the supply pressure crossed a certain second threshold value, the jet started following the contour of the curved surface regardless of any external disturbance. The jet remained stable in this state upto the maximum pressure that could be supplied in the lab

(around 5 psi or 34.5 kN/m²). Thus, this region was named as the *Attached jet region* or the *Wall jet region*.

These three distinct regions where the Coanda jet had distinct flow patterns were noted for all combinations of the other parameters and thus established.

3.2 Interaction of the Coanda air jet with a rigid, stationary web

3.2.1 Experimental setup

In this second stage of experiment, the focus was to study the interaction of the Coanda jet with a rigid, stationary web. The main concern was to find the pressure distribution and the friction force on the rigid web. The measurement of aerodynamic friction is very crucial as it can prove the feasibility of using the in-plane air to handle web materials.

To study the effect of a rigid, stationary web, the setup used for the study of the Coanda air jet in free space was slightly modified. The main additions to the previous setup included a traversing table, a rigid support for suspending the web, a rigid, stationary, web and the instruments used for measuring the force and the pressure distribution.

To simulate a rigid web (E), a thin (0.13 inches or 3.18 mm thick) transparent plexiglass plate was used. Since the rigid web had to be placed in between the two side plates (air dams), its width was maintained at an exact 5.95 inches (151 mm). The parallelism of the two edges of the rigid web was also kept

under a very low tolerance. This was done because the web should not touch the side plates and thus induce a friction component into the load being measured by the load cell. At the same time, if the gap between the web and the two side plates was large, the flow of air through these gaps might affect the measurement. So the web was machined with a high accuracy. The thickness of the rigid web was kept to a minimum so that the effect of the weight of the plate is minimized. If the weight of the plate was considerable compared to the vertical force, then any misalignment of the rigid web hung by the four strings would affect the measurement of the horizontal drag force. Due to the small thickness of the plexiglass plate, bending deformation of the plate became a concern. To minimize the deformation of the rigid web, three pieces of plexiglass (0.5 x 0.5x 18 inches) were fixed lengthwise on the web. Later we found that these three plexiglass rods were not stiff enough, and two aluminum angles were fixed on the web. To measure the pressure distribution along the length of the web, a row of four pressure taps (0.016 inches or 0.41 mm in diameter) were drilled along the center line of the plate with a spacing of 2 inches (51 mm). The holes were drilled carefully and all burrs were removed from the surface of the web without making any scratches, since any irregularity on this surface would affect the pressure reading. The dimensions of the pressure taps are shown in Fig. 3.2.

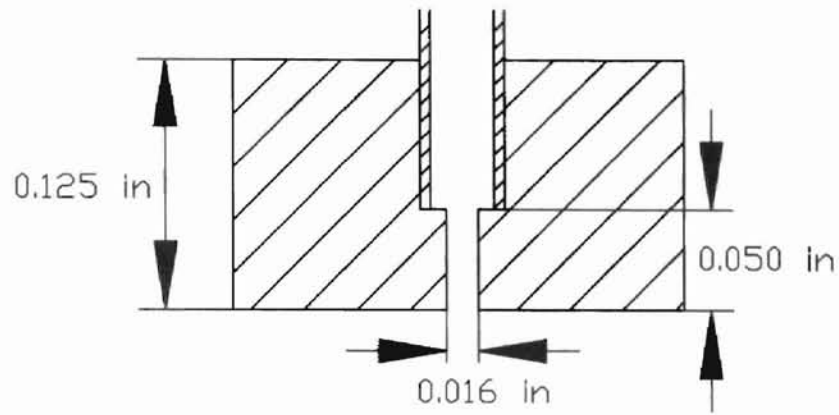


Figure 3.2: Schematic of the pressure taps on the rigid web

One of the easiest methods to measure the horizontal force acting on the web was to fix a strain gage on the web and calibrate it to read the horizontal force. This idea was discarded due to the sensitivity of the standard strain gages available and the difficulties inherent in positioning and connecting the strain gage. Another idea for measuring the force was letting the web hang freely from an overhead support and then measuring the distance by which the web moved from a reference point and then calibrating this distance to correspond to an equivalent force. This method was also discarded due to the aerodynamic pressure on the web which comes into effect by this arrangement. Another inherent inaccuracy of this kind of an arrangement was that if the web moved in the horizontal direction, it would in effect travel in an arc due to the suspending threads. This would affect the vertical flotation height which is a key test variable. The method that was finally proved practical was to use a load cell (K) to measure the horizontal force on the web. The first idea was to fix the load cell on the cantilever beam above the web and connect a projection from the web to

the sensing element of the load cell. This method also had a problem: the vertical forces, which include the gravitational force and the aerodynamic pressure, affected the force on the load cell. Since the load cell was not in the same vertical plane as the web, these vertical forces were in fact making the load sensor to measure a moment value depending on the vertical and horizontal distance between the load cell and the web. Thus the final setup had the load cell positioned in the same plane as the web and on one side of it. The load cell was placed before the nozzle so that the force being measured was the tensile force. The stand, on which the load cell was fixed, also had an arrangement by which the vertical position of the load cell could also be changed so as to position it in the same horizontal position as the web.

For measuring the pressure distribution on the web, a resistive coil type pressure transducer was connected to one of the pressure taps. The pressure could also be read off from a manometer but since we were using a digital data acquisition software (LabVIEW, Release 4.0.1) we needed to obtain the outputs as electrical signals and so we used a pressure transducer that gave the output in the form of DC volts.

To measure the pressure distribution, we had to either move the web, keeping the setup at a certain position or vice versa. Since moving the web might affect the parallelism of the web and the follow-up surface, we decided to move the setup with the help of a traversing table keeping the web at a fixed position. The traversing table (I) is shown in Fig. 3.4. It had a table mounted on

a leadscrew type arrangement with a fixed base. The moving table had two cylindrical guide rods about 0.75 inches (19 mm) in diameter near the two edges. These two rods were fixed firmly to four pillow blocks which were in turn fixed to the bottom base plate. Along the center of the moving table, in between the other two rods, there was also a leadscrew which could be turned by the use of a wheel (H) to move the table. The pitch of the leadscrew was around 18 threads-per-inch and this gave a very good resolution for the movement of the table. A rigid structure made of steel was fixed to the bottom base plate of the table and this was used for suspending the web and the load cell.

Another important design consideration was the method by which the web was suspended from the cantilever beam (C). Since the web was suspended by threads (D), if any of the threads had any angle other than exactly vertical, a horizontal force component would exist. To ensure that the effect on the force measurement was minimized, another aluminum plate (A) was fixed on top of the cantilever beam with the same width as the web and small diameter holes were drilled on the exact same positions as those on the web support beams where the threads were passed through. This arrangement ensured that when the web was suspended, the threads would be exactly vertical. Also to be able to change the flotation height (and also for leveling purposes), an arrangement was used similar to that found in guitars using bolts (B) with holes at the heads. When the bolt was turned, the thread would wind itself around the head, thus increasing the flotation height of the web.

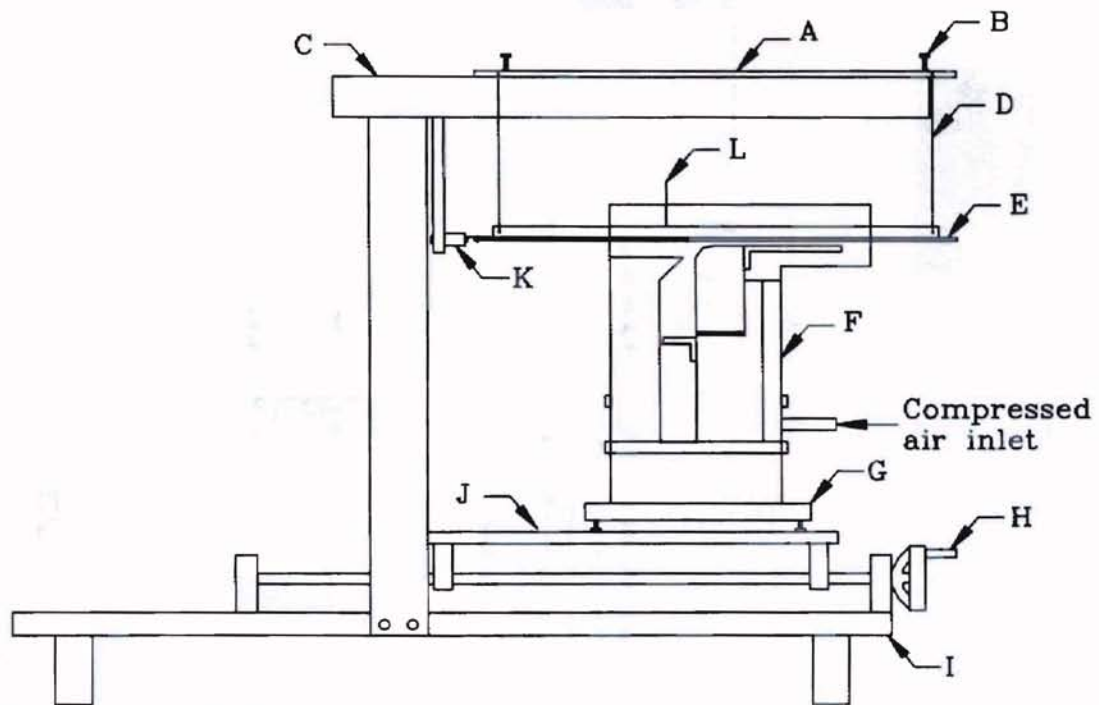


Figure 3.3: Schematic of the setup for the interaction of the Coanda air jet with a rigid, stationary web

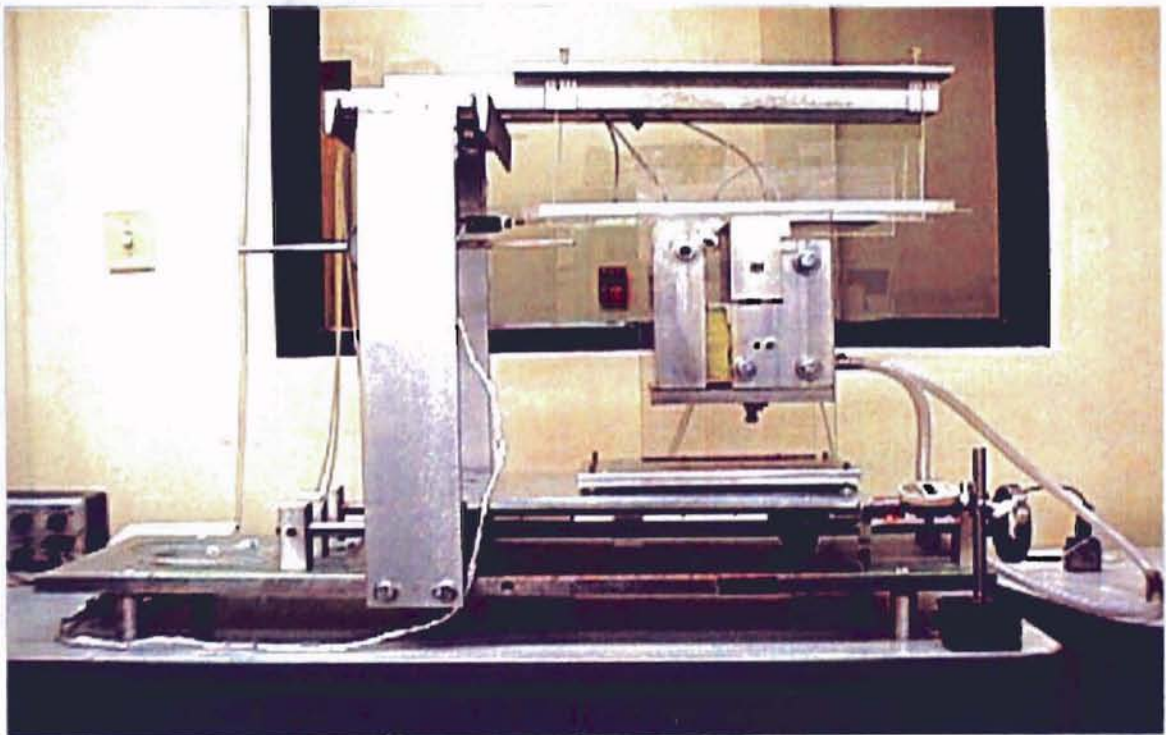


Figure 3.4: Picture (side view) of the setup for the interaction of the Coanda air jet with a rigid, stationary web

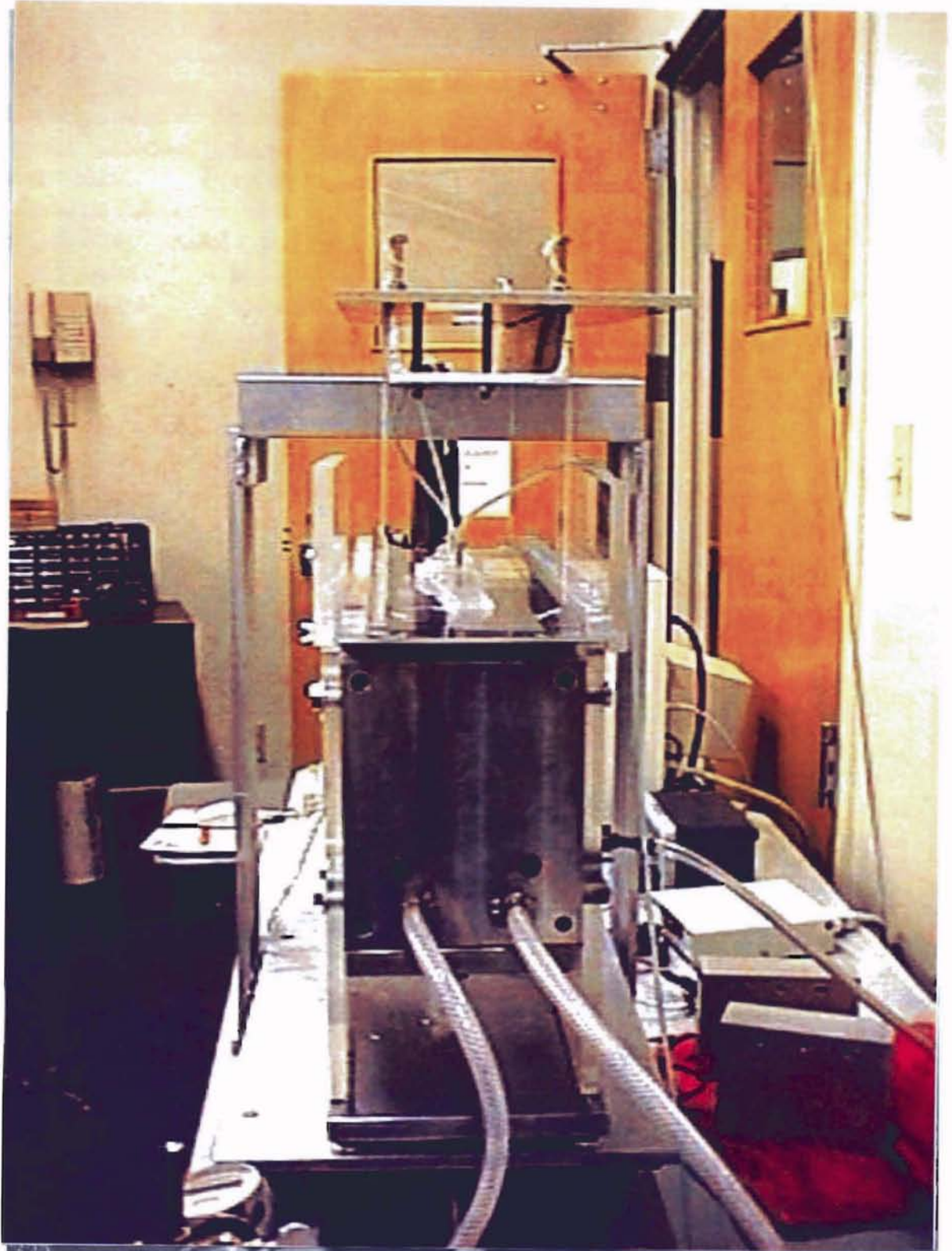


Figure 3.5: Picture (front view) of the setup for the interaction of the Coanda air jet with a rigid, stationary web

Figure 3.4 shows the side view of the actual test setup. The traversing table and the cantilever beam support for hanging the web can be clearly seen. The side view of the rigid web can be seen just above the nozzle and the curved surface blocks. The black rectangle on the left of the web is the load cell. It has been fixed such that it is in the same plane and the same axis as the rigid web. The strings that have been used to suspend the web can be seen in Fig. 3.5. The row of pressure taps and the aluminum struts can also be seen clearly. The four bolts seen at the top are used for adjusting the flotation height of the web with respect to the top parts of the follow-up surface and the curved surface blocks.

3.2.2 Procedure for testing the interaction of the Coanda air jet with a rigid web

The whole setup was placed on the traversing table so that the relative position between the web and the nozzle could be changed easily and accurately. This distance between the nozzle exit and the pressure tap was measured using a digital depth gage. To ensure that the bottom surface of the web and the top surface of the follow-up surface were exactly parallel, we mounted a leveling table on the traversing table and then placed the setup on it. The web was suspended from the overhanging beam using twine. The load cell was also fixed on to a projecting piece of aluminum plate hanging from the above mentioned beam and this formed the rigid base for mounting the load cell. The other end of the load cell was then connected, using some screws, to a projecting piece of

plexiglass that was fixed to the upper surface of the web. Thus when there was any force acting on the web, this same amount of force would act on the load cell and the load cell output would correspond to the force acting on the web.

In this phase of experiments, we used a digital data acquisition system for collecting and storing the data. It had two components: the Analog to Digital converter and the Personal computer. The outputs from the load cell and the pressure transducer were connected to the appropriate pins on the AD converter box. The data acquisition software was configured to be in the differential mode to read all the data. It was programmed to sample around 200 data points and then find the mean of these to get an average value. The outputs were then stored in a text file in the PC itself. This type of data acquisition was used since the data could be obtained more accurately as well as very easily.

Before placing the setup on the traversing table, the values of the various parameters was fixed as done in the previous phase of experiments. Before starting to take any readings, the first thing to be checked was that the center line of the setup was parallel to the center line of the lead screw. This was essential since if it was not so, then as the table was moved, the setup would travel at an angle to the web and then the full horizontal force could not be measured. Next, the parallelism of the web and the top surface of the curved surface block and the follow-up surface was checked and adjusted using some levels and the leveling table if necessary. Another main parameter which was included in this phase was the flotation height of the web, taking the top surface of the follow-up

surface as the reference level. This was set to the required value by either adjusting the length of the twine or by adjusting the leveling table. The horizontal position of the load cell was also adjusted so that the point at which the load was being measured was vertically above the nozzle. Since the nozzle width would be one of the parameters that would be changed, the vertical surface of the curved surface block on the side of the nozzle was taken as the reference and all distances measured to its right were considered to be on the positive axis.

After all the parameters were adjusted and checked, the zero correction for the load cell and the pressure transducer were input into the LabVIEW program. The table was set at a position such that the load cell was vertically above the nozzle. Then the supply air pressure was increased and set at a predetermined value and all the readings were taken using the data acquisition program. The table was moved through a total distance of around 4 inches (in steps of 0.05 inches) and at all the positions the program was run and the data collected.

CHAPTER 4 RESULTS AND DISCUSSION

4.1 Behavior of the Coanda air jet in free space

Experiments have been performed to study the behavior of a Coanda air jet with the surface outside the nozzle having a 90° convex curvature. This is followed by a brief study of the interaction between the air jet and a stationary web, mainly focusing on the pressure distribution on a rigid, stationary web and the horizontal force exerted by the air jet on the web. This study can help in finding optimal values for the geometric parameters of the Coanda nozzle for supporting and transporting the web.

In the first phase of experiments, as mentioned before, there was no web interacting with the Coanda air jet. The behavior of the air jet (for various configurations of the Coanda nozzle) as it exits out of the nozzle was studied so as to arrive at an equation which would predict the behavior of the air jet. The parameters that were thought to affect the behavior of the jet were:

1. Nozzle width (b): This is defined as the horizontal distance between the knife edge of the nozzle block and the vertical face of the curved surface block.
2. Nozzle offset (h): This is defined as the vertical distance between the knife edge of the nozzle block and the starting of the curvature on the curved surface block.
3. Supply air pressure (P): This is the air pressure in the settling chamber measured by a pressure tap on one of the walls.

4. Radius of curvature (R): This is the radius of the edge of the curved surface block that is directly outside the nozzle exit.

The range of values of the various test parameters are tabulated in Table 4.1 .

Table 4.1: Cases considered for the Coanda air jet in free space

Parameter	Symbol	Range	Steps of change
Pressure	P	0 - 2 psi	0.009 psi
Nozzle width	b	0.01 - 0.04 inches	0.005 inches
Nozzle offset	h	0 - 0.20 inches	0.05 inches
Radius of curvature	R	0.078, 0.141, 0.172 inches	

While performing the experiments in the first phase, we noticed that the Coanda jet changed its behavior depending on the combinations of the above named parameters. For example, keeping all others constant, if the supply pressure was slowly increased, the jet first followed a path tangential to the curved surface i.e. it went in a vertical direction not following the curvature of the convex surface. As the pressure was increased farther, and crossed a threshold value, the jet started behaving as a bistable jet where, depending on the way it had been deflected, it would either follow the curvature of the convex surface or it would travel in the vertical direction. As the pressure was increased further, the tendency of the jet to follow the curvature of the surface increased and after crossing another threshold value of pressure, the jet was completely attached to the surface. At this stage, the air jet stayed attached to the curved surface regardless of how it was disturbed. The above mentioned behavioral

patterns of the air jet were studied and it was found that these threshold values of pressure were quite consistent for the configurations tested and none of the patterns changed. So the regions were named after the behavioral patterns as the "Separated Region" (where the air jet was separated from the curved surface and traveled in a vertical path), the "Bistable Region" (where the air jet was either separated from or attached to the curved surface depending on the history) and the "Attached or Wall Jet Region" (where the air jet was attached to the curved surface and followed its contour after exiting out of the nozzle). The existence of these three distinct regions was noticed for all configurations of the nozzle tested.

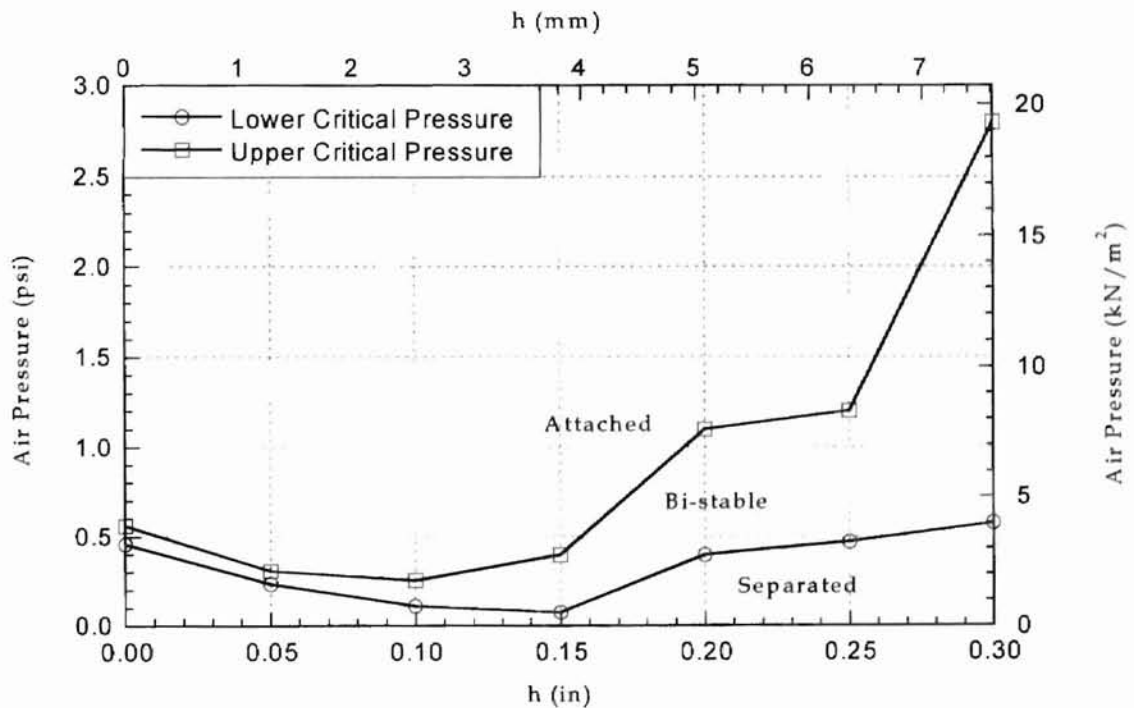


Figure 4.1: Effect of supply air pressure for the Coanda air jet in free space ($R = 0.078$ in, $b = 0.01$ in)

As seen in the above Fig. 4.1, for a height (h) = 0.3 inches (7.6 mm), for supply air pressures below a critical threshold value of 3.4 kN/m^2 (0.5 psi.) , the air jet is always separated from the curved surface. Thus this region has been named as the “Separated Region”. For pressures between 3.4 kN/m^2 (0.5 psi.) and of 19 kN/m^2 (2.75 psi.), the air jet has two stable states: separated from and attached to the curved surface. These two states can be “toggled” by disturbing the air jet. Since it has two stable states, the air jet is said to be in a “Bistable Region”. Above this second critical pressure of 19 kN/m^2 (2.75 psi.), the air jet is always attached to the surface and so it is said to be in an “Attached or Wall Jet Region”.

The existence of these three states or regions for other configurations of the Coanda nozzle was confirmed by further experimentation as seen in Figs. 4.2 and 4.3. These three states were found to have almost the same shape for different combinations of the geometry of the Coanda nozzle and the following curved surface though the critical threshold pressures changed slightly.

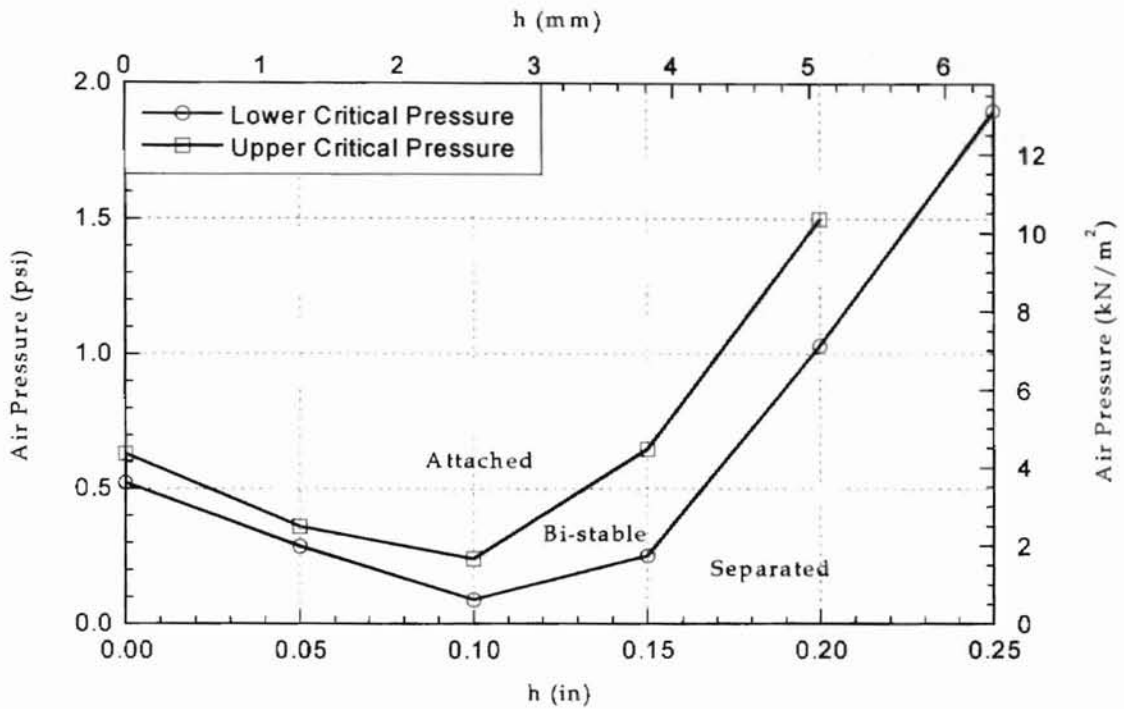


Figure 4.2: Effect of air pressure for the Coanda air jet in free space ($R = 0.078$ in, $b = 0.02$ in)

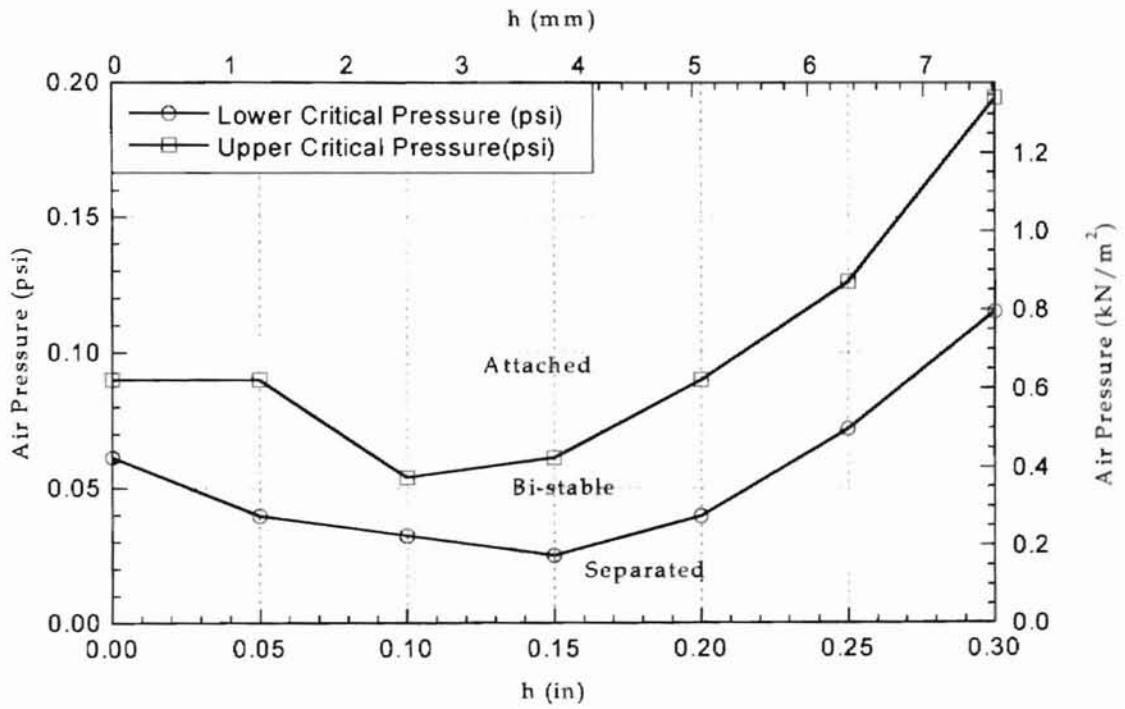


Figure 4.3: Effect of air pressure for the Coanda air jet in free space ($R = 0.141$ in, $b = 0.04$ in)

Another point to be noted is that since we want to find a condition for the attachment of the air jet to the solid surface, only the higher threshold pressures have been considered for all later calculation and plotting purposes. Hence any pressure referred to later in this thesis is the higher threshold pressure.

4.1.1 Effects of nozzle width

The first parameter that was checked for its effect on the behavior of the Coanda air jet was the nozzle width (b). The nozzle width was defined as the horizontal distance between the knife edge of the nozzle block and the vertical edge of the curved surface block. To better understand how the positions of the three regions changed with change in the nozzle width, all the data for the same radius of curvature (R) were plotted on the same graph.

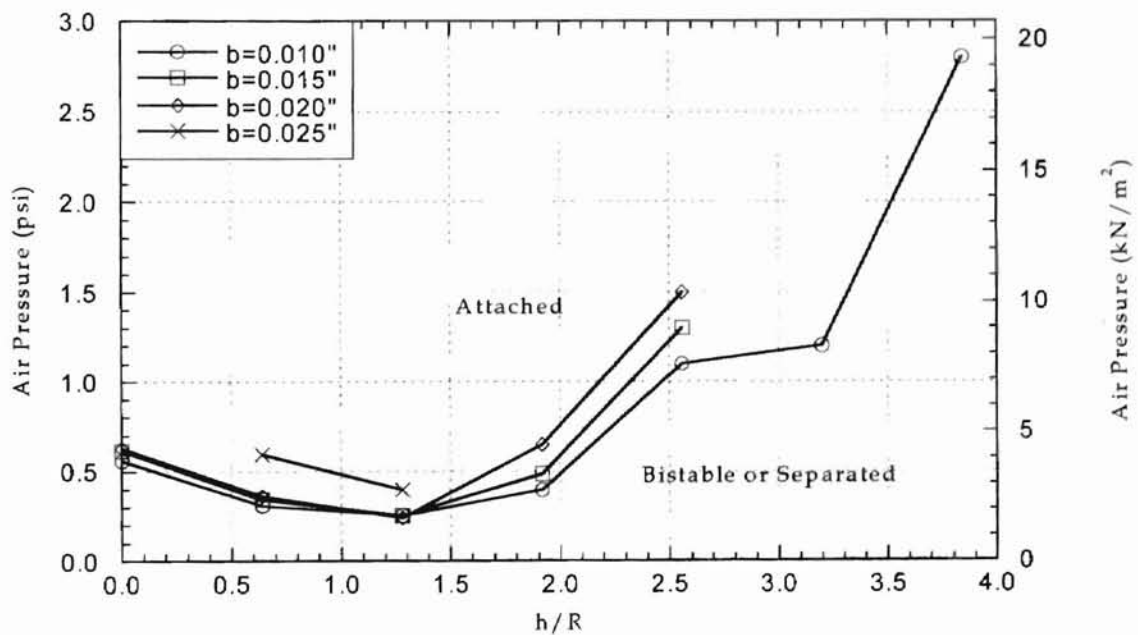


Figure 4.4: Effect of nozzle width for the Coanda air jet in free space ($R = 0.078$ in)

Figure 4.4 shows the data for the effect of change in nozzle width for a radius of curvature of $R = 0.078$ inches (1.981 mm). As seen in the figure, the shape of the boundary between the bistable and the attached jet regions does not change with increase in the nozzle width. Another point to be noted is that the threshold pressures are not strongly affected by the nozzle width. Also the boundaries have the same contours and this led us to believe that there might exist a common function representing the effect of nozzle width. Graphically, this meant that all the lines in the above graph would collapse into one line. To do this, various methods were tested. The first method to bring the lines closer was by taking the natural logarithm of the pressure term. By doing this, the lines did come closer to each other but were still apart. The main concern was to find a function having the nozzle width as a factor, either in the first power or any multiples thereof. When this was tried, the lines did come nearer to each other but they also approached a trivial solution (near zero). Since this was not acceptable, this line of thought was discarded. For the next step we tried using a polynomial function of the nozzle width. Since the easiest was a first order polynomial, we tried with this first. In any first order polynomial, there are two terms, one coefficient and one constant. Since we were trying to find a polynomial function, we resorted to a shortcut: fixing one term (the constant) as being equal to one. By doing this, the number of unknown values was reduced from two to one. After this, changing the value of the coefficient, we could arrive

at one particular value giving the best fit between the various data sets and collapsing all into a single line. Figure 4.5 shows the end result after this series of algebraic manipulations.

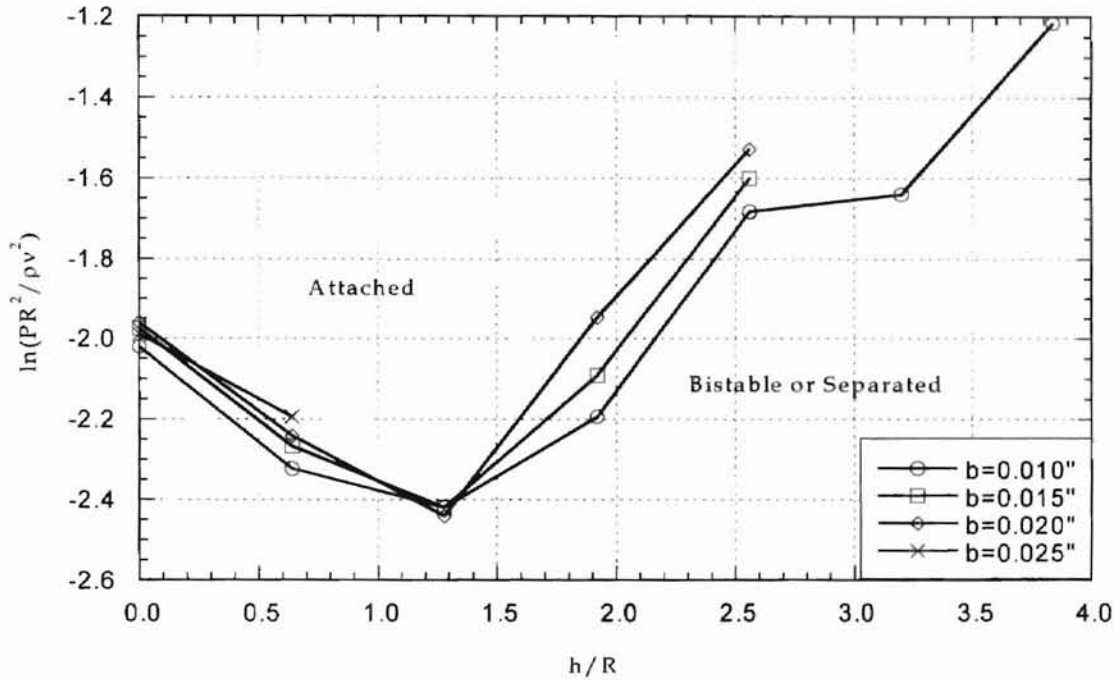


Figure 4.5: Effect of nozzle width for the Coanda air jet in free space ($R = 0.078$ in) after manipulations

As seen in Fig. 4.5, the data sets almost collapse into one single line. Any further increase or decrease from this value of the coefficient makes the sets move apart. The data lines do not become a single line showing that there are more factors which have to be combined to get the required end result.

4.1.2 Effects of nozzle offset

One of the other main factors governing the behavior of the air jet seemed to be the vertical height between the top of the nozzle block and the top of the curved surface blocks (which we call as h). Following the same procedure as before, we plotted the non-dimensional width against the non-dimensional pressure and then plotted the data for various h values on a single graph and this is shown for one case in Fig. 4.6 ($R = 0.078$ inches or 1.981 mm).

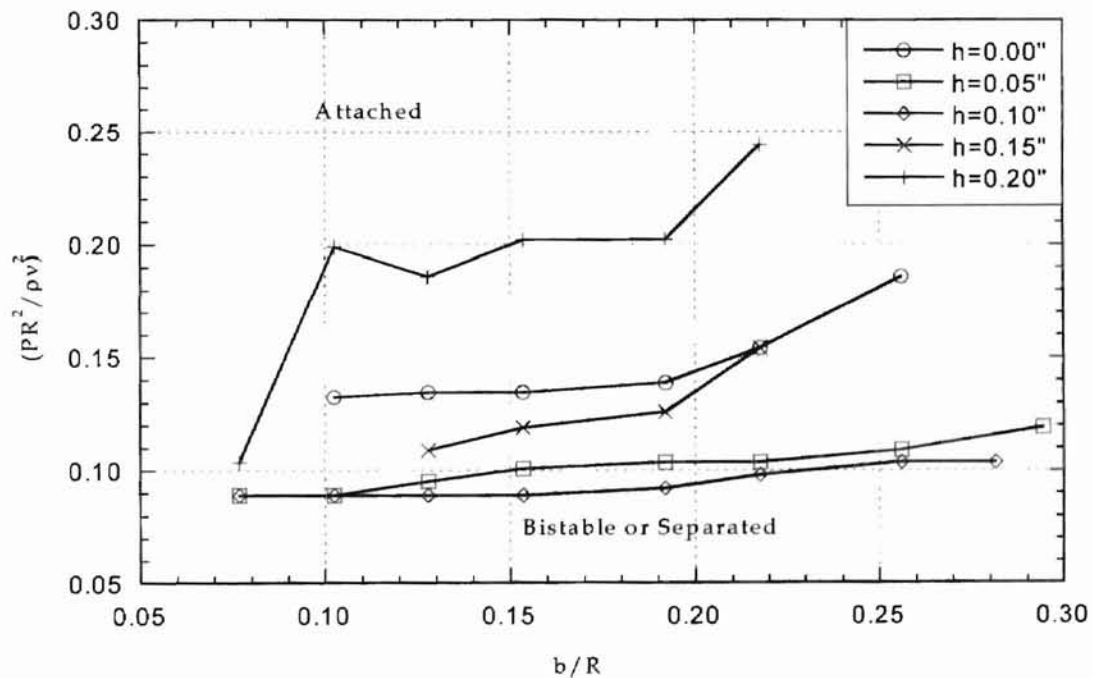


Figure 4.6: Effect of nozzle height for the Coanda air jet in free space ($R = 0.078$ in)

As seen in Fig. 4.6, the nozzle offset does have a considerable effect on the behavior of the air jet. Here again, the shapes of the data lines do not change a

lot indicating that the effect of the nozzle height might be close to linear. The same data for a different value of radius of curvature is shown in Fig. 4.7.

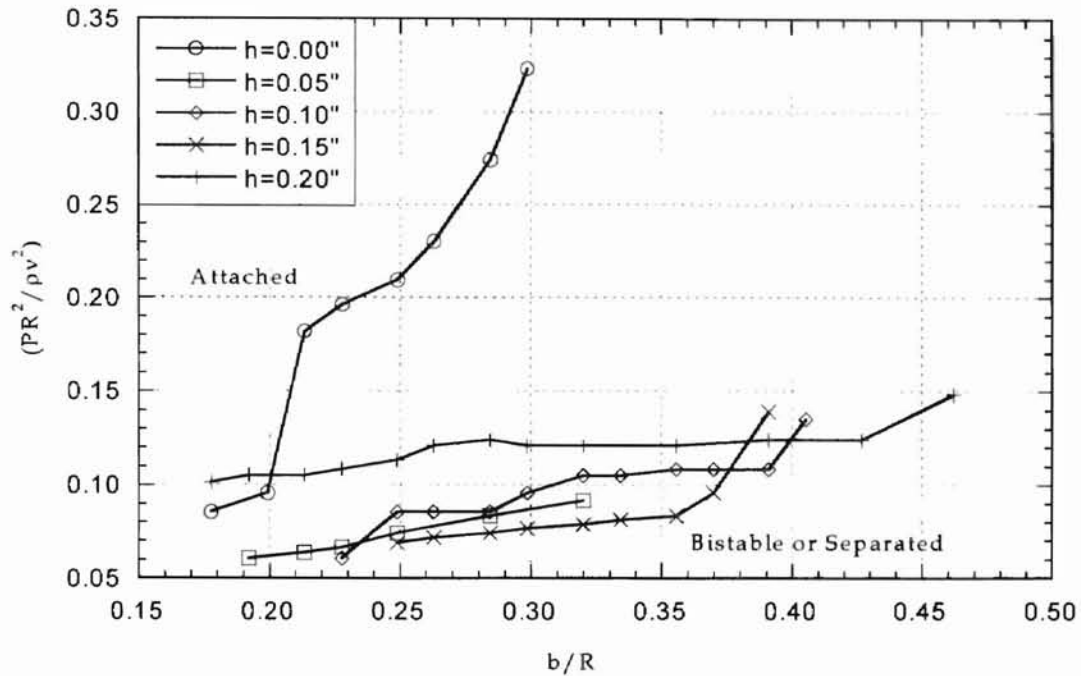


Figure 4.7: Effect of nozzle height for the Coanda air jet in free space ($R = 0.141$ in)

In Fig. 4.7, the shape of the curve for $h = 0$ inches is a little different from the others. One important trend to be noticed from both these graphs is the way the pressure drops from $h = 0$ inches till around $h = 0.10$ inches (2.540 mm) and then reverses and starts rising after $h = 0.150$ inches (3.810 mm). This trend is very pronounced in the previous graph (Fig. 4.6). This trend indicates that there might exist a range of critical heights within which the lowest critical pressure required for the air jet to become attached is very low. Any value of h out of this range would increase the pressure required for the attachment of the jet. When we tried to collapse these lines into a single line following the same procedure as

for the effect of nozzle width, we found that this does not work due to the peculiar trend exhibited by the nozzle offset. Thus we conclude that there exists a critical range of h (between 0.05 inches and 0.15 inches) within which the supply pressure required for the air jet to attach to the curved surface is minimum.

4.1.3 Effects of radius of curvature

The radius of curvature of the curved surface following the nozzle is one of the foremost in importance when studying the Coanda effect. The effect of the radius of curvature was also studied for the behavior of the Coanda air jet in free space.

The radii of the three blocks tested were 0.078 inches, 0.141 inches and 0.172 inches. The data when plotted for the three radii while keeping all the other parameters constant looked as shown in Fig. 4.8.

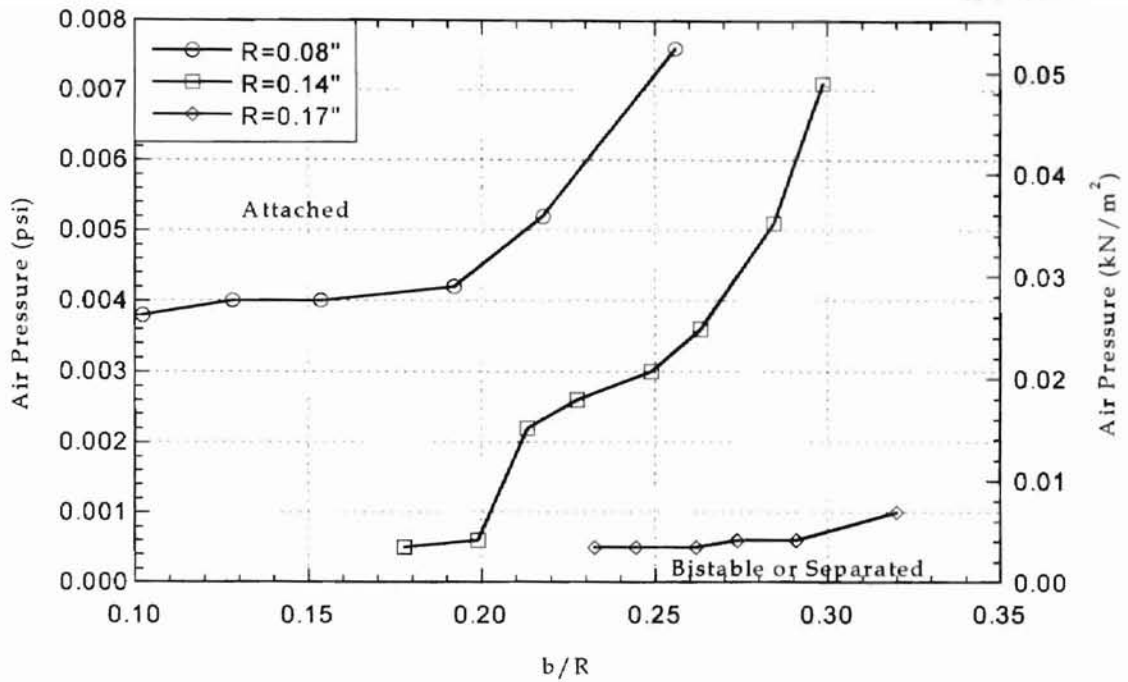


Figure 4.8: Effect of radius of curvature for the Coanda air jet in free space ($h = 0.000$ in)

As seen in Fig. 4.8, the critical pressures for the attachment of the air jet to the curved surface decreases rapidly as the value of the radius of curvature is increased. This is in conjunction with the theory that as the curvature is increased, the Coanda effect is more pronounced and the supply air pressure required for attachment is decreased. The same trend was noticed in all experiments for different values of h and b . Thus we can say that as the radius of curvature of the solid surface is increased, the required critical pressures become lower.

4.2 Interaction of the Coanda air jet with a rigid, stationary web

The aim of this phase of experiment was to find whether the air jet can deliver enough friction force useful for lateral position control and other web handling applications.

The parameters considered for these experiments were the same as before with only one addition. The flotation height (h_1) of the web, which was defined as the vertical distance from the top surface of the follow-up or curved surface block to the bottom surface of the rigid web, was also taken into consideration here. The main parameters are the supply air pressure, the nozzle width and the flotation height. Since the Coanda air jet will follow the rectangular path defined by the web, the follow-up surface and the two end plates, in this part of experiments, the air jet will have a channel flow.

The range of values of the test variables are tabulated in Table 4.2

Table 4.2: Cases considered for the interaction of the Coanda air jet with a rigid, stationary web

Parameter	Symbol	Range	Steps of
Pressure	P	8-16 in H ₂ O	4 in H ₂ O
Nozzle width	b	0.025-0.040 inches	0.05 inches
Nozzle height	h	0 inches	
Radius of curvature	R	0.172 inches	
Flotation height	h_1	0.12, 0.15, 0.18 inches	0.03 inches

In this phase, the pressure distribution and the friction drag were of the main concern. A typical pressure profile is shown in Fig. 4.9.

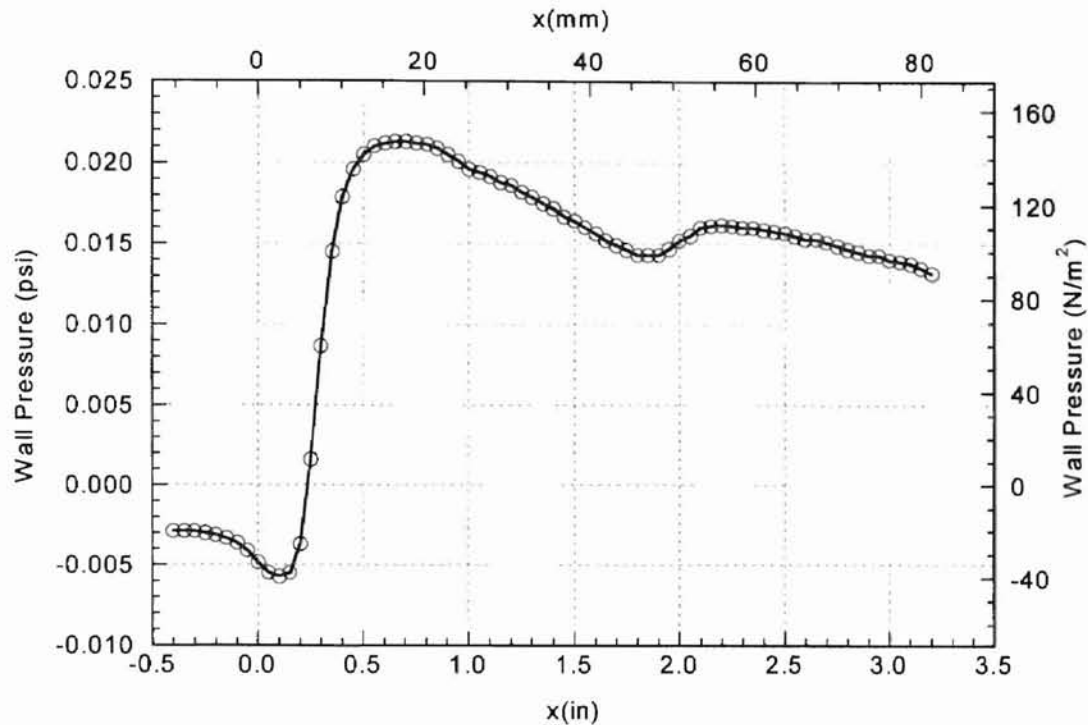


Figure 4.9: Pressure profile on the rigid web ($R = 0.172$ in, $b = 0.030$ in, $h = 0.000$ in, $h_1 = 0.150$ in, $P = 12$ in H_2O)

As seen in Fig. 4.9, the pressure profile on the left of the nozzle exit is below the ambient pressure. Therefore air is entrained into the main stream of air jet in that region. The small drop of pressure even below this negative pressure just after the nozzle is due to the sudden turning of the air jet direction. This creates a low pressure area above the air jet and below the rigid web. At this stage, it should be remembered that the air jet thickness might be just a little more than the nozzle width: certainly not equal to the flotation height that was tested. This creates a vacuum between the air jet and the web and so this might cause the dip in the pressure profile. Within a very short distance, due to the pulling force of the vacuum pressure existing above it and due to its own

momentum, the air jet's width increases tremendously and becomes equal to the flotation height. This accounts for the sudden shoot-up in pressure just to the right of the nozzle. After the air jet width stabilizes, the pressure profile reaches a plateau and then starts to slowly decrease toward the ambient pressure. This happens due to the escaping of the air jet out of the constricted region between the nozzle and the rigid web. As the pressure decreases, there is another rise which is seen in the pressure profile just around 1.5 inches (38 mm) from the nozzle. This might be caused due to either one of two reasons. The first one is that the air jet might not have become completely stabilized, and due to the phenomenon of attachment as described by Murai and others (1989), it might be oscillating between the two solid surfaces (the rigid web at the top and the follow-up surface at the bottom). This might cause a small vacuum region to be created at either wall when it separates from it. The second reason might be the build-up of back pressure at this point. As the air jet moves along the rectangular path, its momentum is slowly reduced. Since the air is being let into the system with a certain inlet pressure, this reduction in momentum causes a high local pressure. Due to the air beyond the follow-up surface exiting into a large open area, the pressure build-up also starts to reduce and become equal to the ambient pressure.

Figure 4.10 shows the friction drag exerted by the air jet on the rigid web.

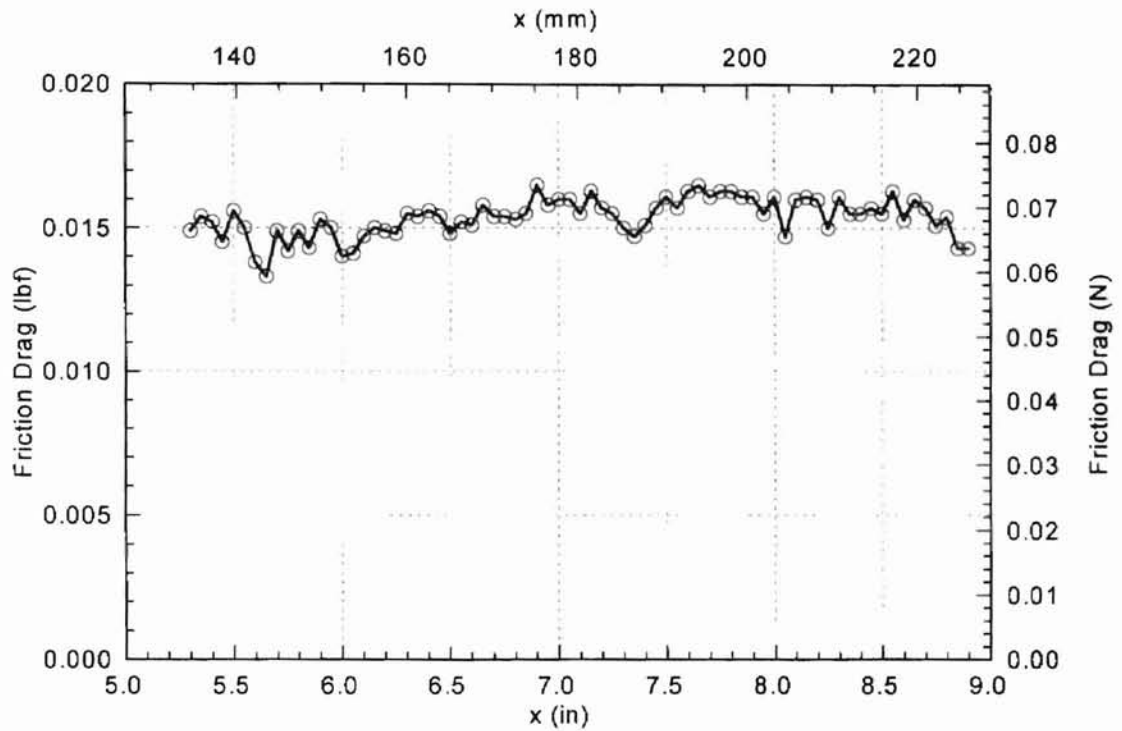


Figure 4.10: Friction drag on the rigid web ($R = 0.172$ in, $b = 0.030$ in, $h = 0.000$ in, $h_1 = 0.150$ in, $P = 12$ in H_2O)

As explained later, the load values being shown by the load cell are an average value of all the local friction drag loads. This is the reason the above profile is an almost straight line.

4.2.1 Effects of supply air pressure

4.2.1.1 Pressure profiles

The supply air pressure was changed for various combinations of all the other parameters. The pressures tested were 8, 12 and 16 inches of water. Figure 4.11 shows the effect of change in supply air pressure on the pressure profile for one configuration of $R = 0.172$ inches (4.369 mm).

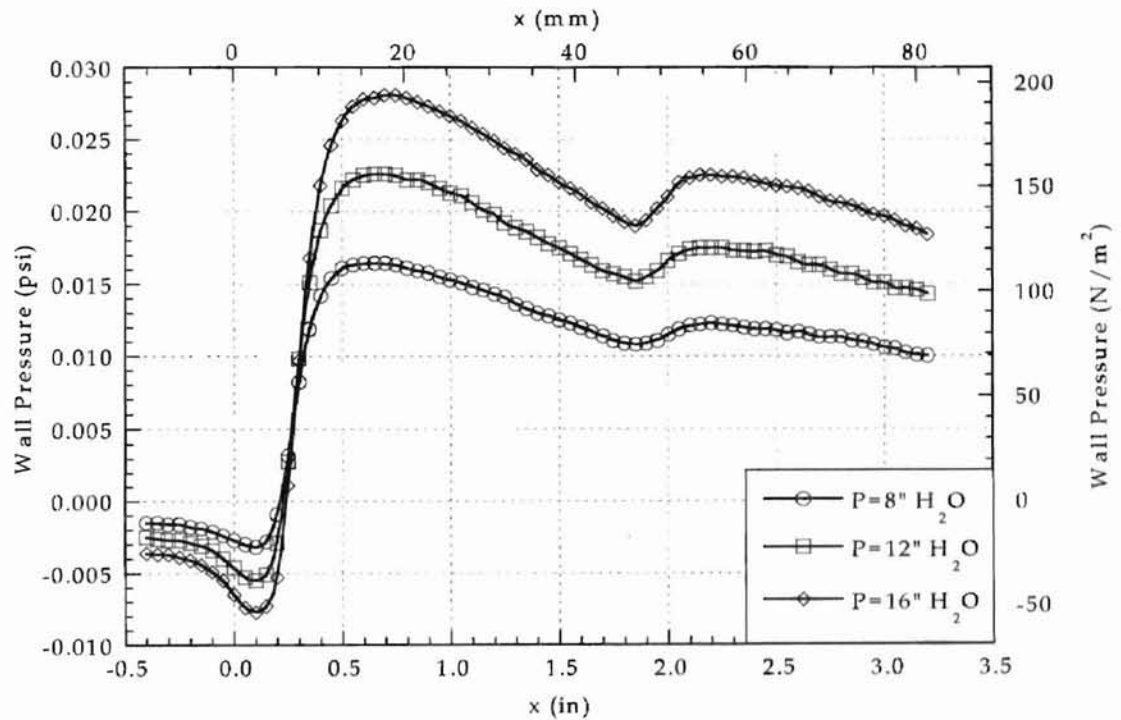


Figure 4.11: Effect of supply air pressure on pressure profile ($R = 0.172$ in, $b = 0.035$ in, $h = 0.000$ in, $h_1 = 0.150$ in, $h_1/b = 4.29$)

As seen in Fig. 4.11, the shape of the pressure profiles do not change with any increase or decrease in the supply air pressure. The only changes occur in the absolute magnitudes of the pressure. As the supply air pressure is increased from 8 inches of water to 16 inches of water, the flow velocity and the volume of flow are increased which makes the peaks and troughs in the pressure profile to be more sharply defined when compared to the profile from any lower supply pressures. This trend and the shape of the pressure profiles was almost constant for all the other configurations that were tried. Due to the increased volume flow of air, the pressure profile of the test for 16 inches of water is more clearly defined when compared to the profile for 8 or 12 inches of water. Figures 4.12 and 4.13 show the pressure profiles for two other configurations.

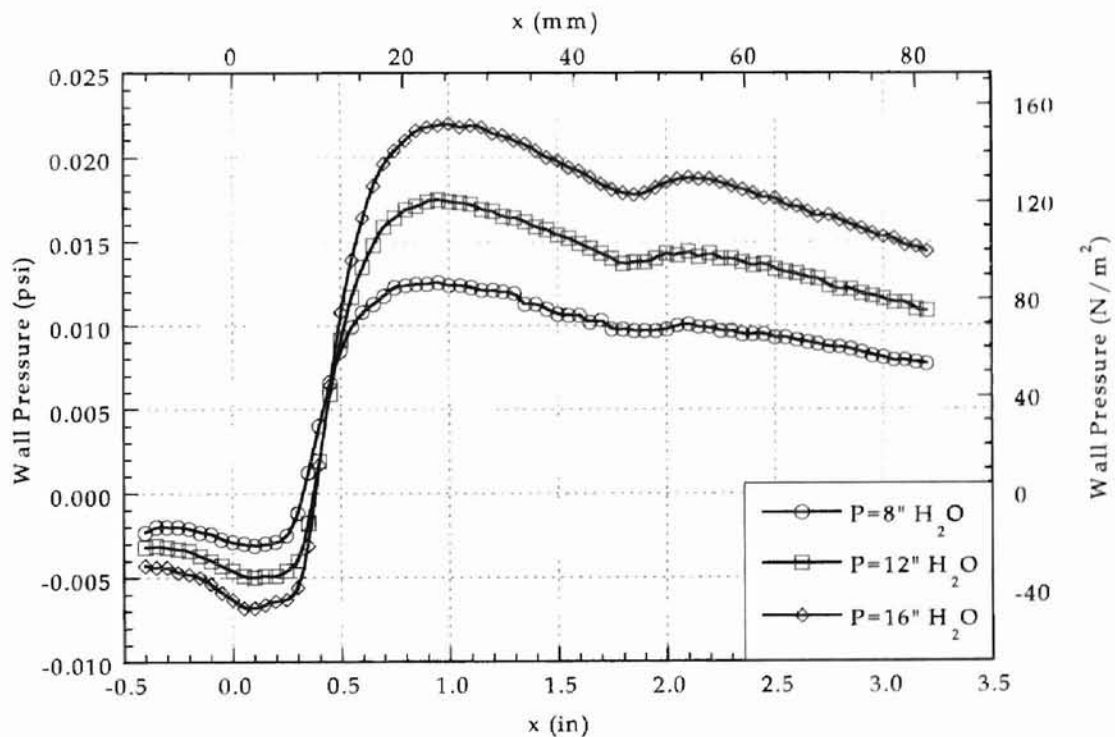


Figure 4.12: Effect of supply air pressure on pressure profile ($R = 0.172$ in, $b = 0.025$ in, $h = 0.000$ in, $h_1 = 0.180$ in, $h_1/b = 7.20$)

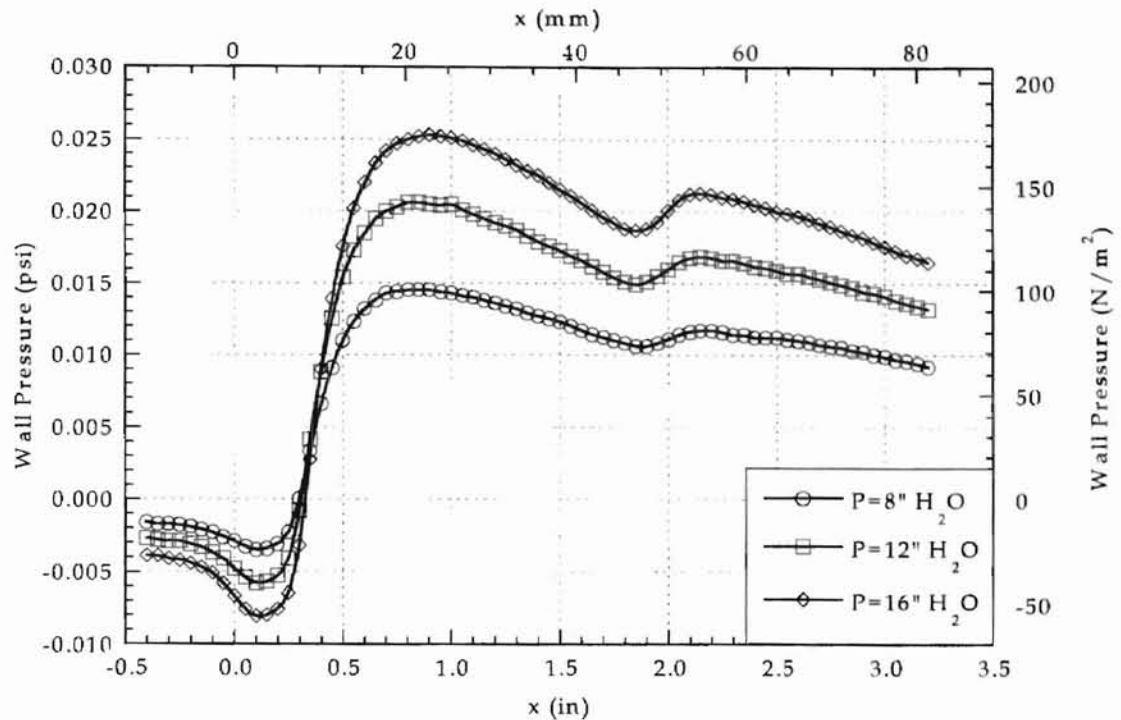


Figure 4.13: Effect of supply air pressure on pressure profile ($R = 0.172$ in, $b = 0.040$ in, $h = 0.000$ in, $h_1 = 0.180$ in, $h_1/b = 4.50$)

4.2.1.2 Aerodynamic friction drag

Figure 4.14 shows the effect of change in supply air pressure on the aerodynamic friction drag for one configuration of $R = 0.172$ in. As seen in Fig. 4.14, the friction drag remains almost constant. By theory, there will exist various local frictional drag values due to the air flow under the rigid web for different relative positions of the nozzle and the load sensor. These will be different from the load cell output as the load cell will give only the mean or resultant of these drags due to inflexibility of the web. This is one major cause of limitation in these sets of experiments. As regards the magnitudes of these average drag values, they are seen to increase with increase in the supply air pressure. This may be due to the increased volume flow which will increase the

velocity of the air because the area of the channel remains constant. Even though the average frictional force seems to increase with any increase in the supply air pressure, it might have a peak value above which the change in the drag may not be considerable when compared to the change in the supply air pressure. Thus the difference decreases gradually and after some value might not increase at all.

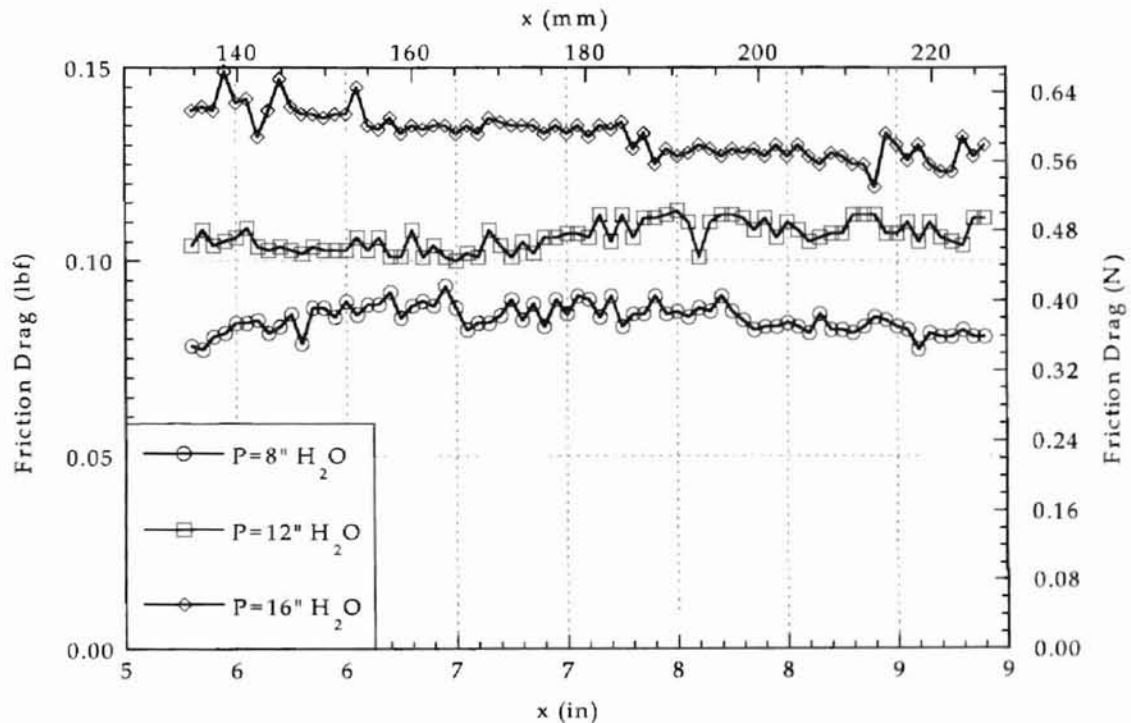


Figure 4.14: Effect of supply air pressure on friction drag ($R = 0.172$ in, $b = 0.035$ in, $h = 0.000$ in, $h_1 = 0.180$ in, $h_1/b = 5.14$)

This trend of the friction drag was observed for other geometries as well, two of which are shown in Figs. 4.15 and 4.16.

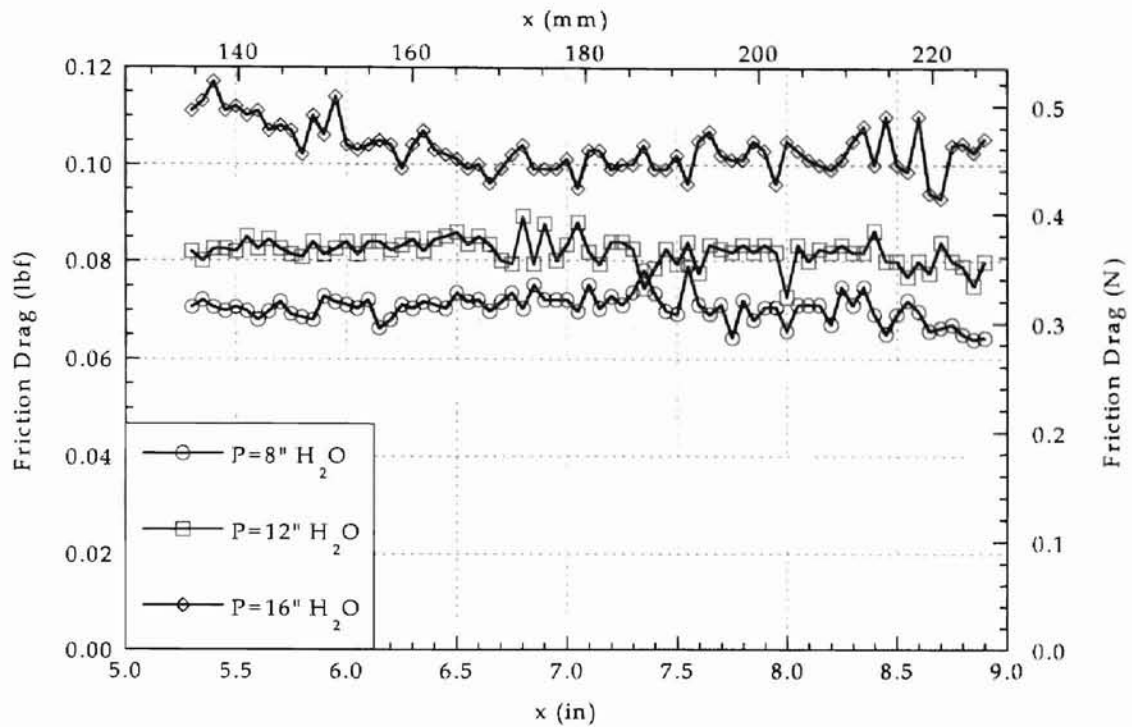


Figure 4.15: Effect of supply air pressure on friction drag ($R = 0.172$ in, $b = 0.025$ in, $h = 0.000$ in, $h_1 = 0.180$ in, $h_1/b = 7.20$)

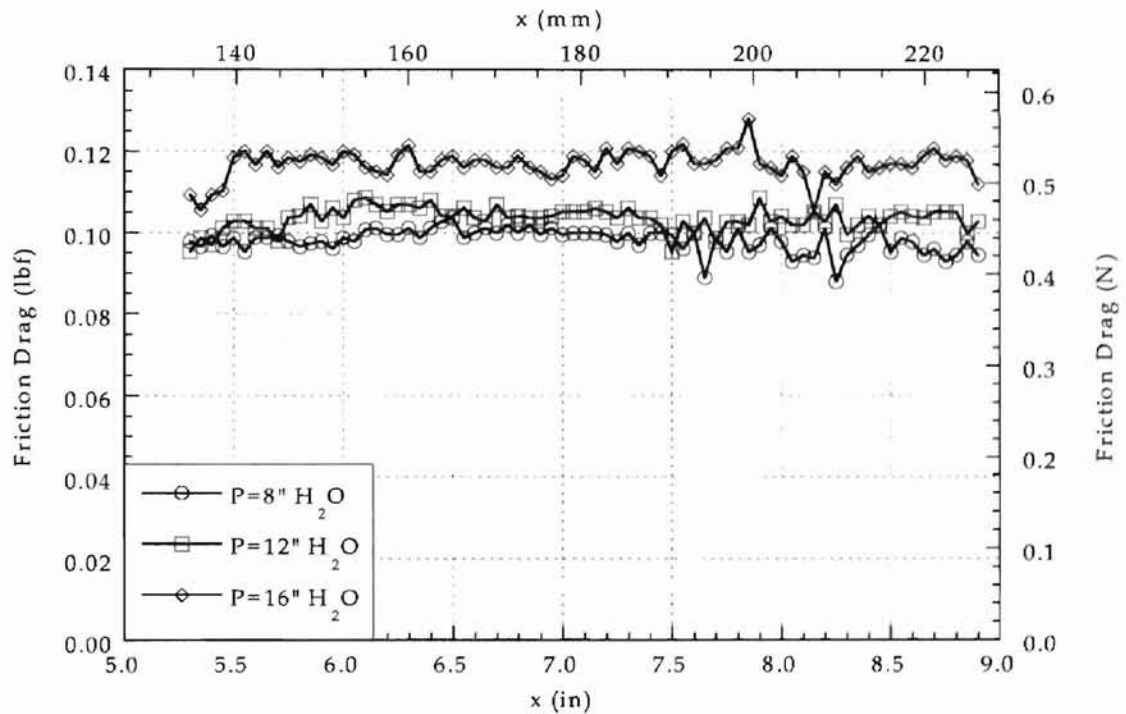


Figure 4.16: Effect of supply air pressure on friction drag ($R = 0.172$ in, $b = 0.040$ in, $h = 0.000$ in, $h_1 = 0.180$ in, $h_1/b = 4.50$)

4.2.2 Effects of flotation height of the web

4.2.2.1 Pressure profiles

The flotation height of the web was changed for various combinations of all the other parameters. The flotation heights tested were 0.12 inches (3.00 mm), 0.15 inches (3.81 mm) and 0.18 inches (4.57 mm). Figure 4.17 shows the effect of change in flotation height on the pressure profile for one configuration of $R = 0.172$ inches (4.37 mm).

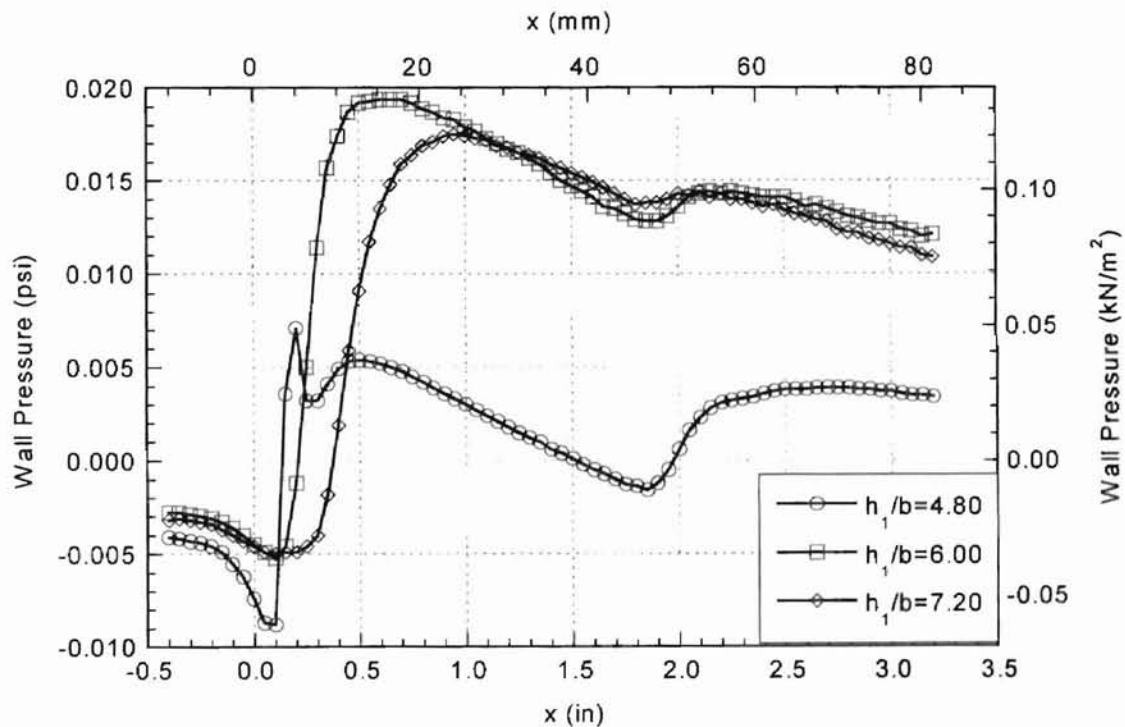


Figure 4.17: Effect of flotation height on pressure profile ($R = 0.172$ in, $b = 0.025$ in, $h = 0.000$ in, $P = 12$ in H_2O)

As seen in Fig. 4.17, the pressure profiles have a dramatic change when the flotation height is changed. For the case where the flotation height is just around 0.12 inches (3.05 mm), the pressure profile is quite low. At the flotation

height of 0.12 inches, there is seen a dip followed by a small peak just before the nozzle exit. This might be due to the fact that the rectangular path defined might be too small for the expanding air jet and so some of the air gets deflected in the opposite direction. Due to the air entrainment properties of the Coanda air jet, the entrained air might conflict with the oppositely deflected air jet thus causing in a recirculation zone being created just before the nozzle. This peak is not clearly seen in the pressure profiles for flotation heights of 0.15 inches (3.81 mm) and 0.18 inches (4.57 mm) which might mean that the width of the expanding air jet was sufficiently accommodated into the flotation height and so the recirculation zone was absent. Thus we can see that as the flotation height is decreased below a certain value a recirculation zone is created. This might also have an effect acting opposite to the desired goal and so must be avoided at all costs. The same kind of trend is noticed for the graph shown in Fig. 4.18.

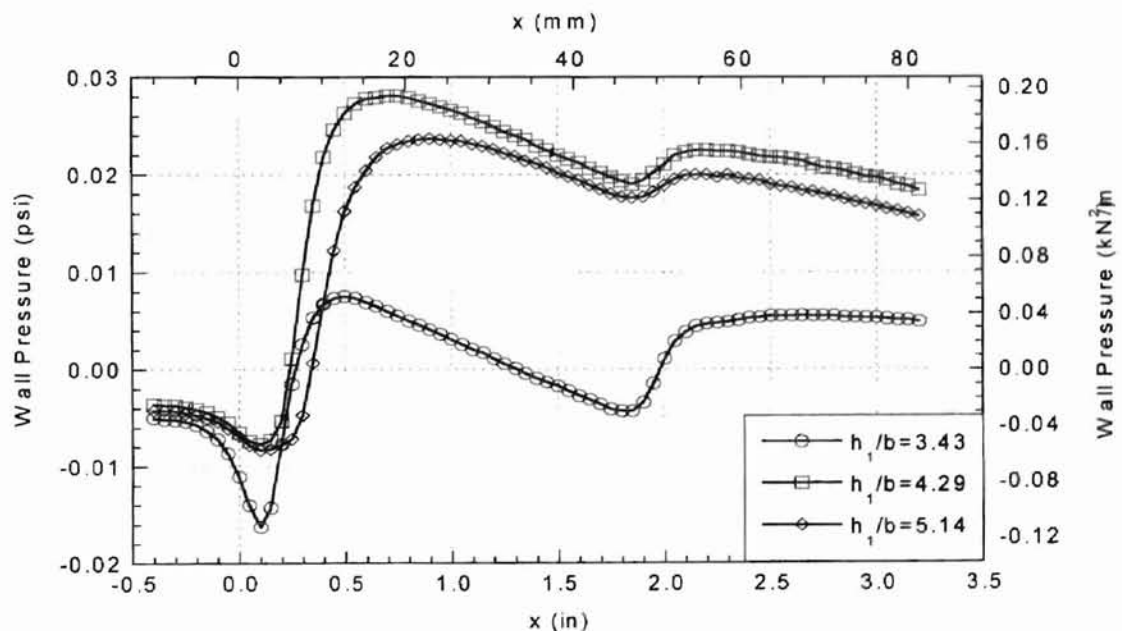


Figure 4.18: Effect of flotation height on pressure profile ($R = 0.172$ in, $b = 0.035$ in, $h = 0.000$ in, $P = 16$ in H_2O)

4.2.2.2 Aerodynamic friction drag

The effect of change in the flotation height on the friction drag exerted by the air jet on the rigid web is discussed in this section. The flotation heights tested were 0.120 inches (3.048 mm), 0.150 inches (3.810 mm) and 0.180 inches (4.572 mm).

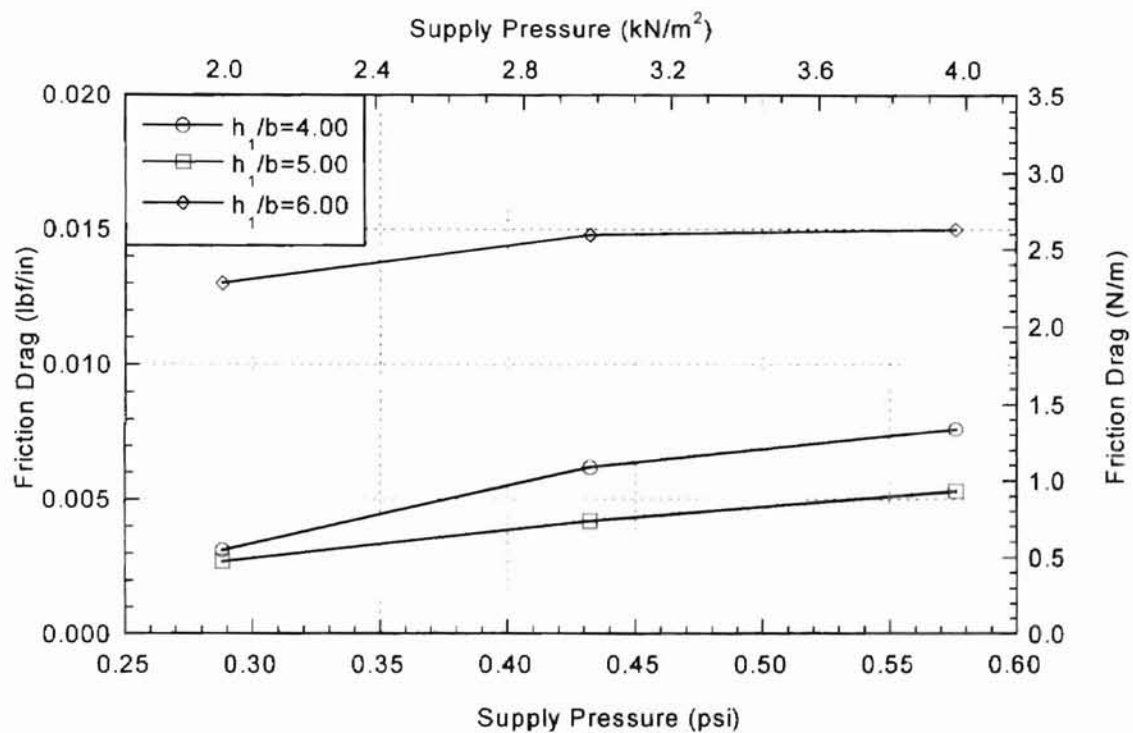


Figure 4.19: Effect of flotation height on friction drag ($R = 0.172$ in, $b = 0.030$ in, $h = 0.000$ in)

As seen in Fig. 4.19, the average friction drag forces have been plotted against the supply air pressures. As seen in Fig. 4.19, friction drag seems to generally increase with increase in the flotation height. This might indicate that the optimum flotation height is above $h_1 = 0.18$ inches. By theory, for all flotation

heights above the optimum value, the frictional drag decreases below that for the optimal height. This is because the volume of flow of air remains constant while the area through which it flows is increased. This effect is believed to act only within a range of flotation height beyond which either the flotation height is too high to exert a considerable amount of force or the flotation height is too low and thus the air jet is deflected in the opposite direction. This same trend is seen in the next figure (Fig. 4.20) for a different value of nozzle width.

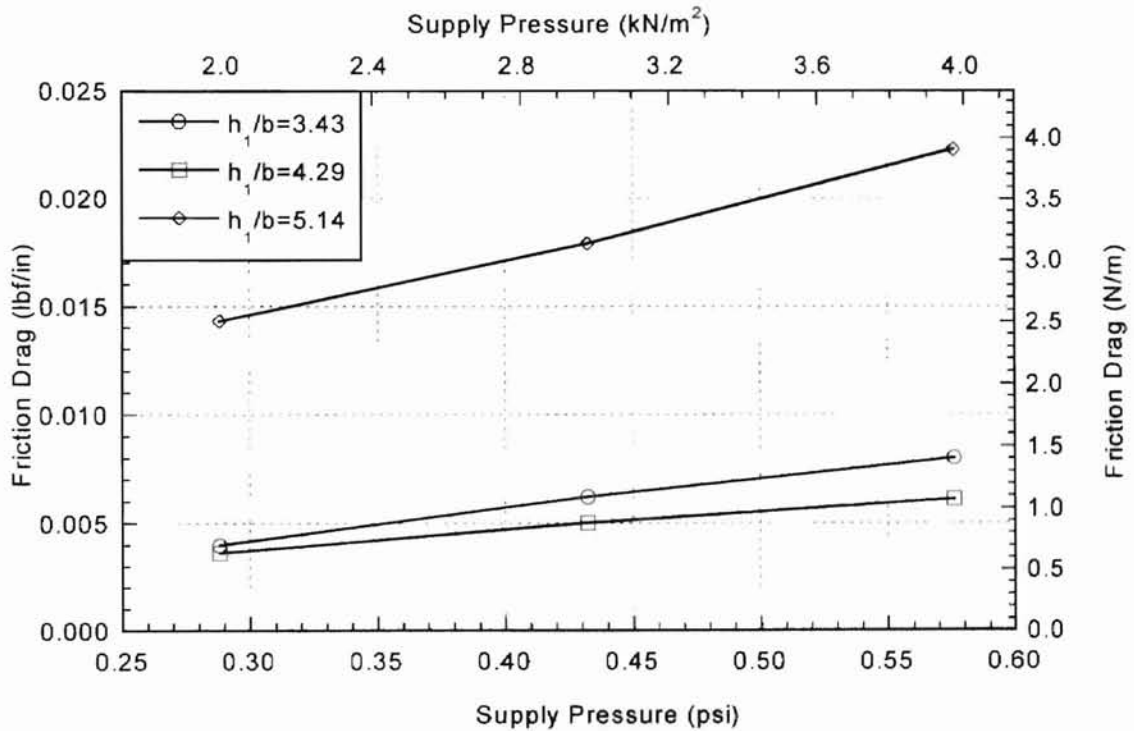


Figure 4.20: Effect of flotation height on friction drag ($R = 0.172$ in, $b = 0.035$ in, $h = 0.000$ in)

4.2.3 Effects of nozzle width

4.2.3.1 Pressure profiles

The width of the nozzle exit was changed for various combinations of all the other parameters. The nozzle widths tested were 0.025 inches (0.635 mm), 0.030 inches (0.762 mm), 0.035 inches (0.889 mm) and 0.040 inches (1.02 mm). Figure 4.21 shows the effect of change in nozzle width on the pressure profile for one configuration of $R = 0.172$ inches (4.37 mm).

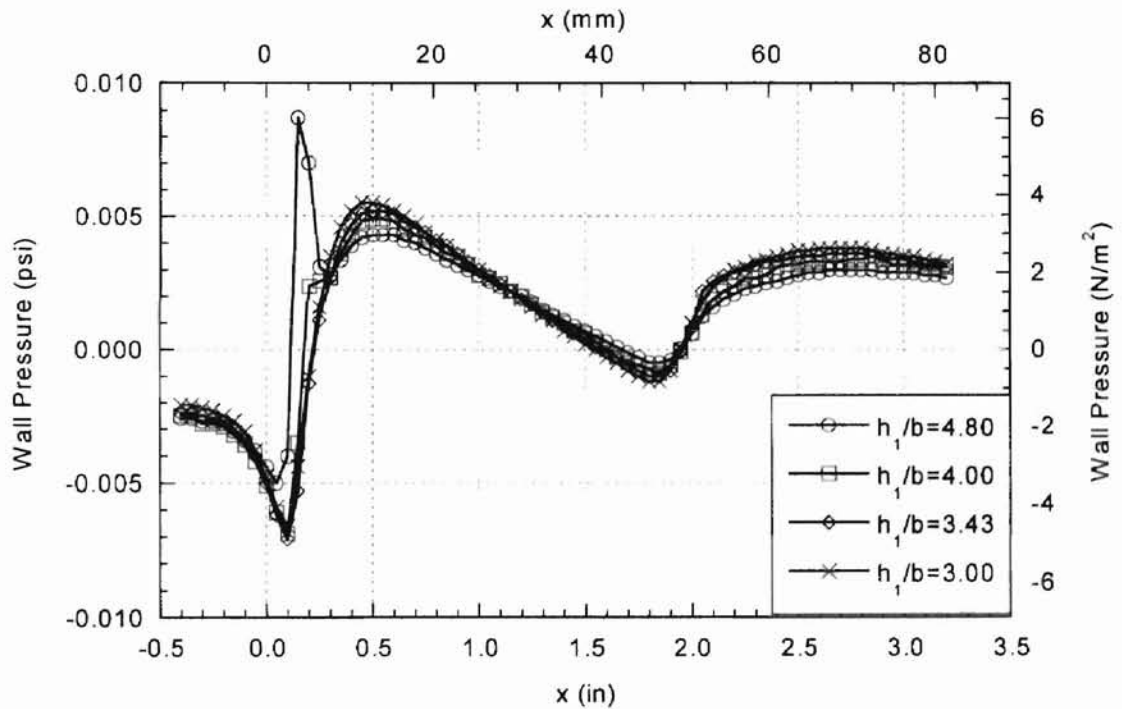


Figure 4.21: Effect of nozzle width on pressure profile ($R = 0.172$ in, $h = 0.000$ in, $P = 8$ in H_2O , $h_1 = 0.120$ in)

As seen in Fig. 4.21, the pressure profile is not much affected by the value of nozzle width used. The only discrepancy from the general trend is the small spike just before the nozzle. This might be due to the previously explained

reason. The same trend can be seen for other graphs as well: one of them is shown in Fig. 4.22.

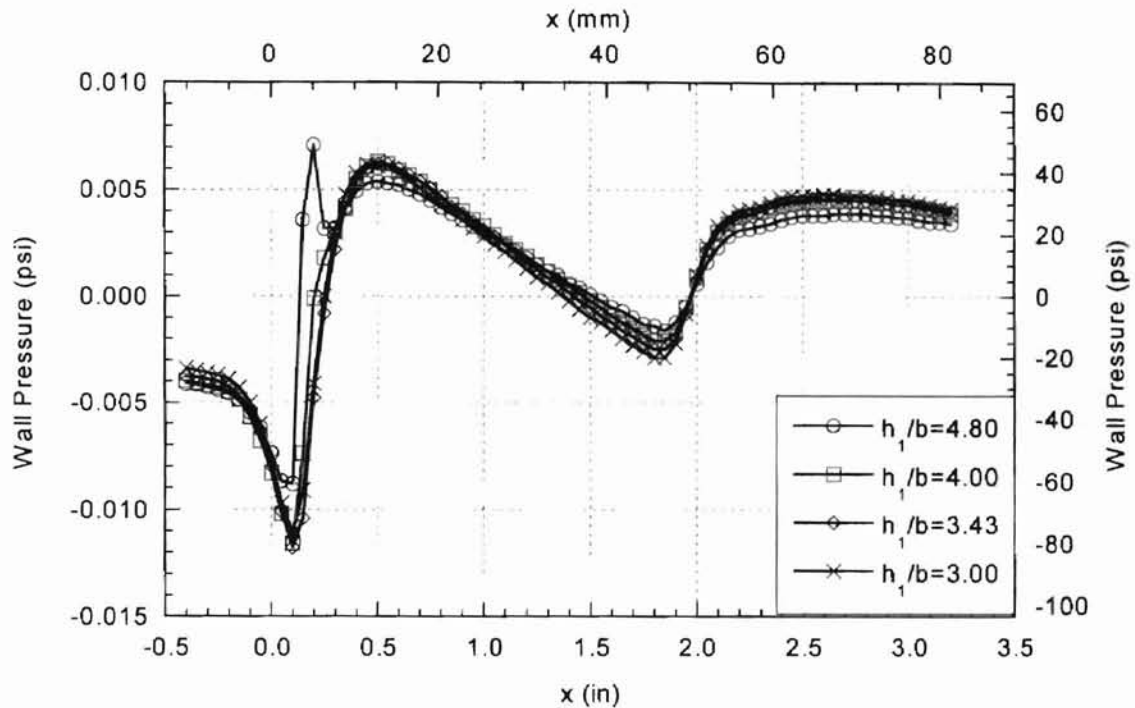


Figure 4.22: Effect of nozzle width on pressure profile ($R = 0.172$ in, $h = 0.000$ in, $P = 12$ in H_2O , $h_1 = 0.120$ in)

4.2.3.2 Aerodynamic friction drag

As seen in Fig 4.23, the average frictional drag increases with increase in the nozzle width because the nozzle width is the main parameter that influences the width of the air jet and thus its behavior. This is because the amount of air exiting out of the nozzle is increased as the nozzle width is increased and this has a direct effect on the friction force. The value of the nozzle width is also believed to have an optimum value above which the air jet starts losing its pressure and

thus will not be able to support the web. This trend was noticed in the other plots as well, one of which is shown in Fig. 4.24.

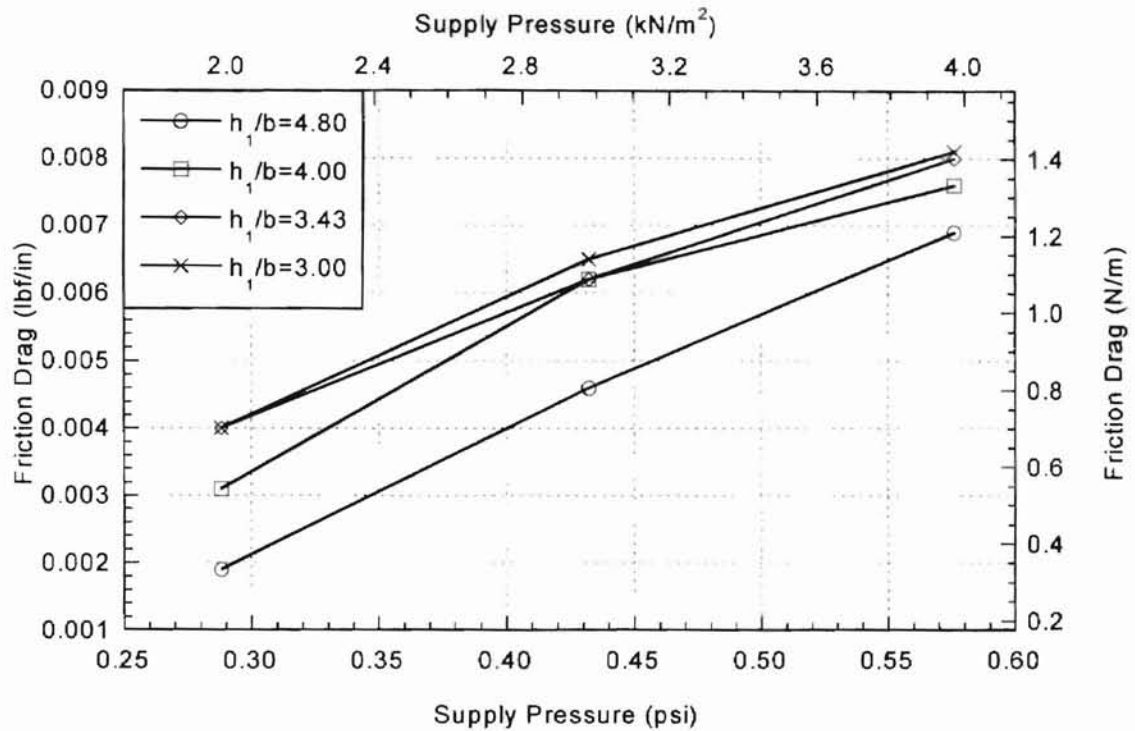


Figure 4.23: Effect of nozzle width on friction drag ($R = 0.172$ in, $h = 0.000$ in, $h_1 = 0.120$ in)

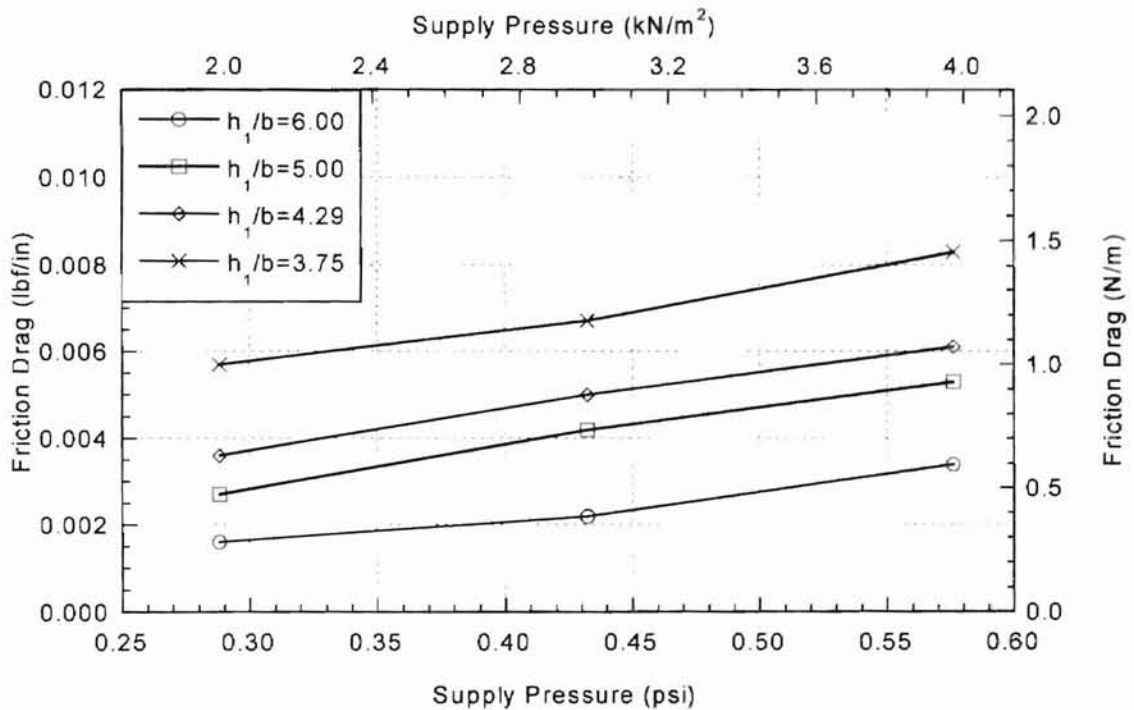


Figure 4.24: Effect of supply air pressure on friction drag ($R = 0.172$ in, $h = 0.000$ in, $h_1 = 0.150$ in)

4.3 Discussion and Comparison with other's study

The present experimental study is compared with the computational study done by Thirumal (1998). Figure 4.25 shows the effect of change in the nozzle width data that were obtained experimentally as well as computationally. As can be clearly seen from the graph, the trends noticed were the same from both methods. It must be noted that the trends could be compared only for the same conditions for both cases and so only the overlapping region can at present be correlated. The same kind of match can be noticed in Fig. 4.26 .

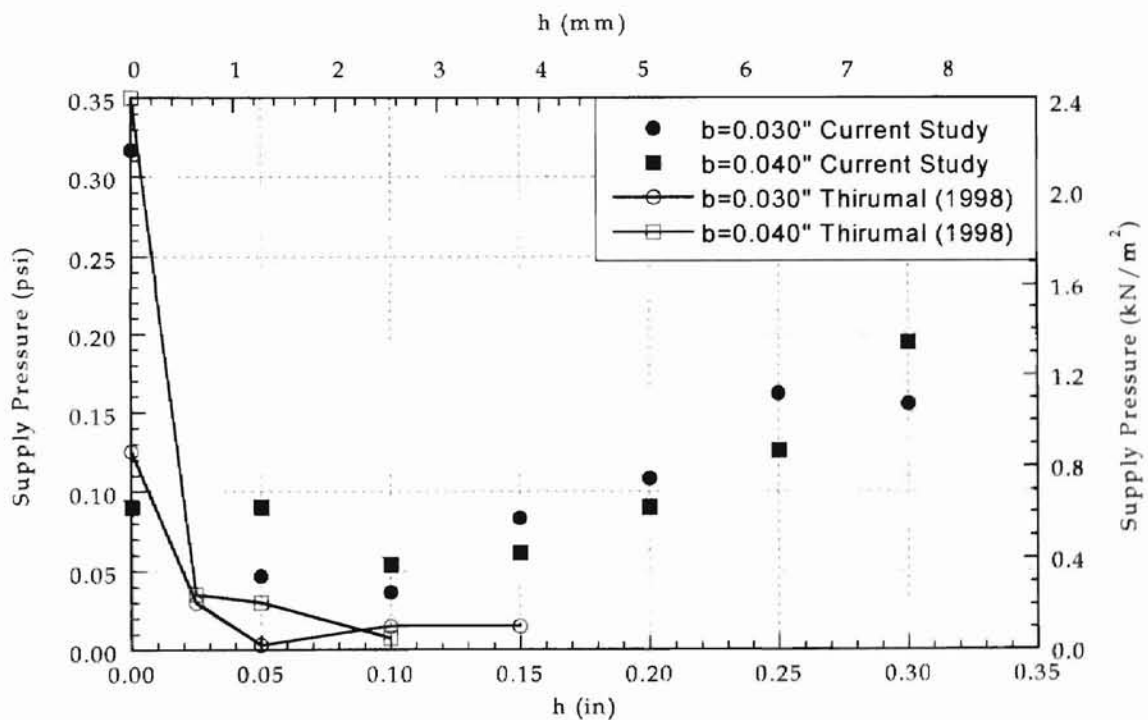


Figure 4.25: Comparison of current experiments with computational results by Thirumal (1998) for the Coanda air jet in free space (Effect of b for $R = 0.141$ in)

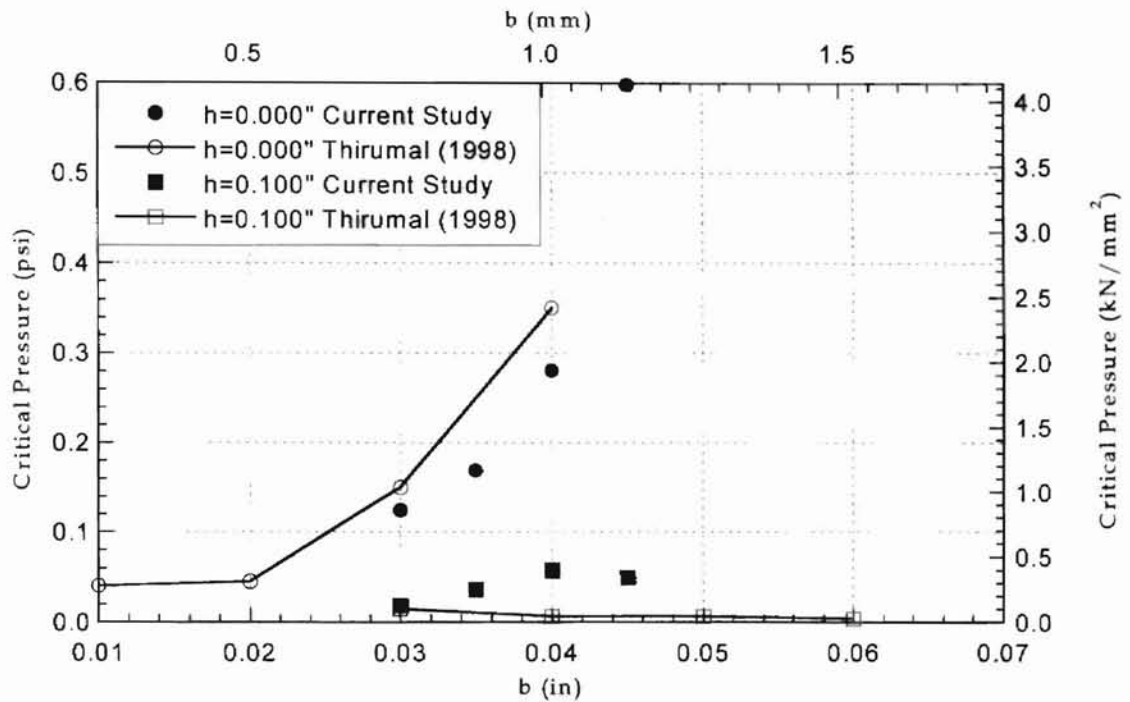


Figure 4.26: Comparison of current experiments with computational results by Thirumal (1998) for the Coanda air jet in free space (Effect of h for $R = 0.141$ in)

The experimental and computational data were also checked for the second phase of experiments namely, the interaction of the Coanda air jet with the rigid web. Since the limitation of the experimental study was that the value of frictional drag obtained was an average value this could not be directly compared to the local shear stress obtained computationally. Instead we have attempted to compare directly just the pressure profiles for the same configurations. The results of this comparison are shown in the following figures.

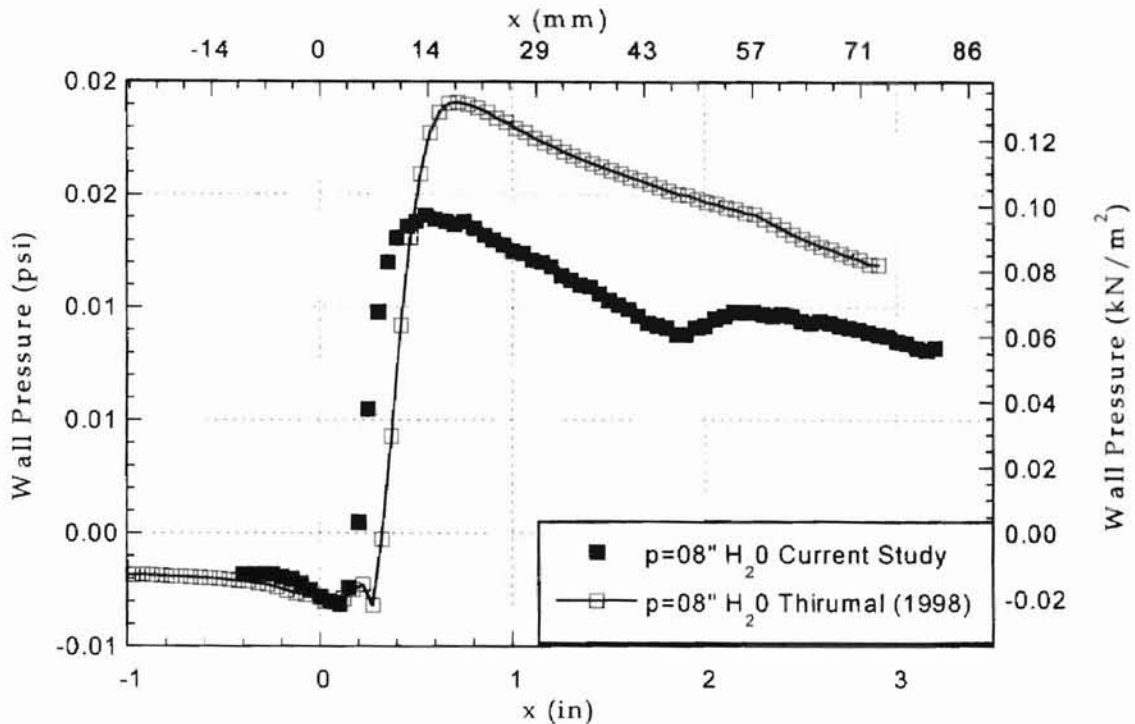


Figure 4.27: Comparison of current experiments with computational results by Thirumal (1998) for the interaction of the Coanda air jet with a rigid web ($R = 0.172$ in, $b = 0.025$ in, $h = 0.000$ in, $h_1 = 0.150$ in, $P = 8$ in H_2O , $h_1/b = 6.00$)

In Fig. 4.27, the pressure profiles obtained by the two methods are seen to clearly match to a very good degree. The reason for the slight difference between the two data are due to the difference in the methods used. In the experimental method, there was an intentional air gap at the side of the jet between the web and the plexiglass side-plates. This could not be avoided due to the friction factor coming into play when measuring the force. In the computational method this type of air gap (leakage) was not considered at all. In this way, the computational method seems to be better. But, practically, there was a problem with the computational method too. To obtain very accurate data, the mesh or grid size of the model had to be extremely small. This increased the calculation

time and thus the instability tremendously. If the program had been allowed to run for more time, the computational model would have yielded more accurate results. Some more graphs comparing the experimental and computational data are shown below (Fig. 4.28).

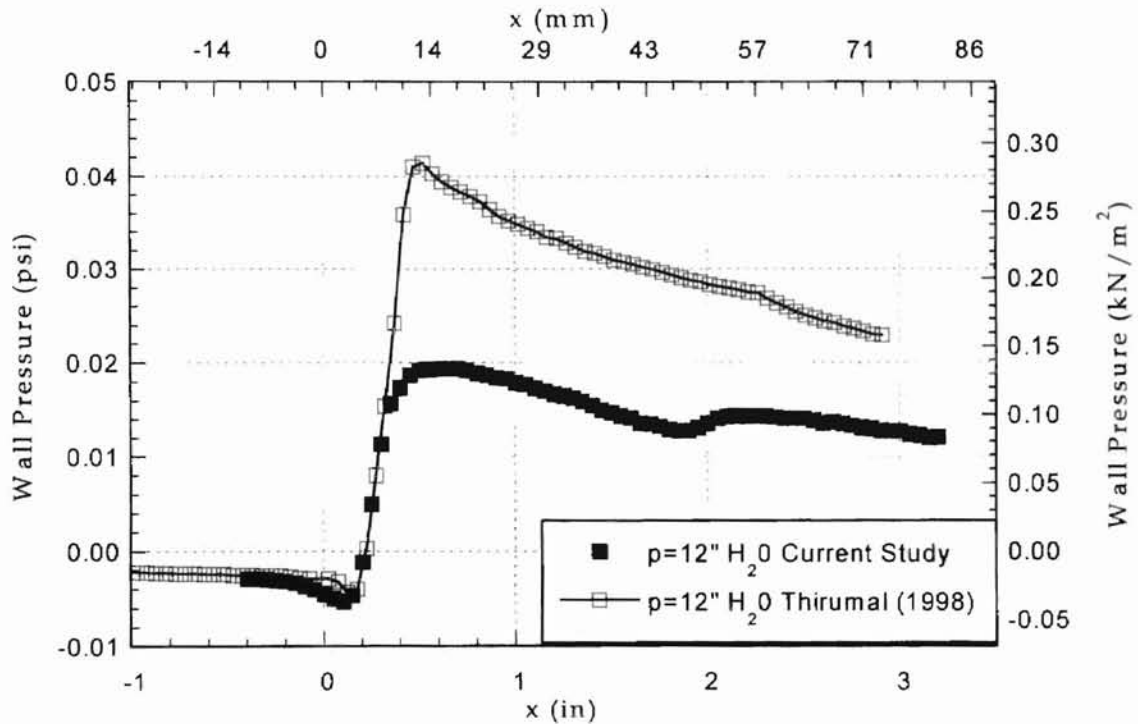


Figure 4.28: Comparison of current experiments with computational results by Thirumal (1998) for the interaction of the Coanda air jet with a rigid web ($R = 0.172$ in, $b = 0.025$ in, $h = 0.000$ in, $h_1 = 0.150$ in, $P = 12$ in H_2O , $h_1/b = 6.00$)

The friction drags that were obtained computationally gave the local frictional forces acting on the bottom surface of the rigid web. Since the drag values obtained experimentally were average values, the computational results were integrated over the surface of the web and the average drag was calculated. These were then compared with the corresponding values obtained experimentally. Figure 4.29 shows a comparison between the experimental data and the computational results obtained by Thirumal (1998).

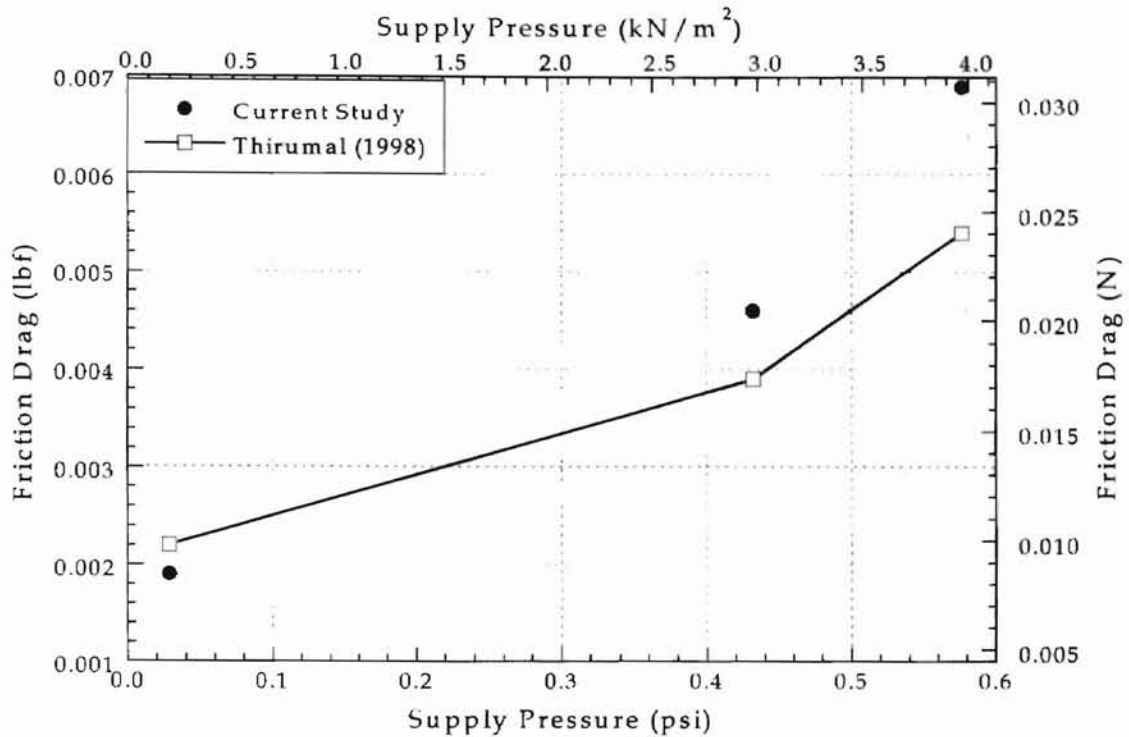


Figure 4.29: Comparison of current experiments and computational results by Thirumal (1998) for the interaction of the Coanda air jet with a rigid web ($R = 0.172$ in, $b = 0.025$ in, $h = 0.000$ in, $h_1 = 0.150$ in, $P = 8$ & 12 in H_2O , $h_1/b = 6.00$)

As seen in Fig. 4.29, the average value of frictional drags for a pressure of 8 inches of water match to very good degree. The average drag calculated from the computational results decreases for the higher values of the supply air pressure. This is because the computational model considered a value of zero for the surface roughness for the bottom surface of the rigid web. This was not so in the experimental case.

4.4 Uncertainty of the experimental data

In the first phase of experiments, all the numerical values of the parameters were measured with the help of shims or distance gages. The values

of the radii of curvature were rounded to the nearest third decimal place since that was the accuracy of the gages used. The pressure measurements were done pretty accurately with the help of well calibrated manometers (with a resolution of 0.1 inches of water) minimizing the occurrence of parallax. This value when converted to pounds-per-square-inch gave a very high degree of accuracy. The method of deflection of the air jet was rather crude but it served the purpose of finding the critical pressures. As explained earlier, the direction of travel of the air jet could not be accurately note for supply air pressures below 0.5 inches of water. Also the increments considered for finding the critical pressures was around 0.25 inches of water.

In the second phase of experiments, the same distance gages were used for determining the values of the geometry parameters. The movement of the traversing table was measured using a digital meter with an accuracy of 0.0005 inches (0.0127 mm) which was well below the steps chosen, 0.05 inches (1.27 mm), during the course of this experiment. The axes of the leadscrew, the test setup, the rigid web, the load cell and the cantilever beam were aligned using some very accurate levels and tri-squares. Express care was taken to avoid these becoming misaligned while handling the test setup and if in any doubt, all these were checked for accuracy. The level of the web and the top surfaces of the curved surface block and the follow-up surface were checked constantly with the help of various liquid levels. The flotation height was checked using distance gages as well as verniers whenever possible. Due to the use of electronic data

acquisition systems, all the components were periodically checked for calibration accuracy. There was also a lot of electronic noise which we tried to eliminate by using adequate shielding for all the wires, etc. Zero corrections were checked and adjusted before any experimentation. While performing the experiment, the fluctuation of the supply air pressure was maintained below 0.2 inches of water. The whole experimental process was conducted within an environmentally controlled zone to minimize the effect of change in ambient temperatures, etc.

CHAPTER 5

ANALYSIS OF EXPERIMENTAL DATA

5.1 Dimensional Analysis

For studying any kind of phenomenon, we use various kinds of basic equations coupled with boundary condition equations. To study lots of such equations based on some dimensional parameters is very difficult. So we often resort to reducing a number of dimensional variables into a smaller number of dimensionless groups. The scheme given here was proposed by Buckingham and is famously known as the *Buckingham Π Theorem*.

The first part of the Π theorem explains what reduction in variables to expect:

If a physical process satisfies the PDH and involves n dimensional variables, it can be reduced to a relation between only k dimensionless variables. The reduction $j = n - k$ equals the number of variables which do not form a Π among themselves and is always lesser than or equal to the number of dimensions describing the variables.

The various steps involved in non-dimensionalizing the equations are :

- List and count the number of n dimensional variables involved in the problem.

- List the dimensions of each variable using the basic parameters $\{M, L, T\}$.
- Find j . Initially guess j equal to the number of different dimensions present, and look for j variables which do not form a Π product. If no luck, reduce j by 1 and look again.
- Select j scaling parameters which do not form a π product. Make sure they have some form of generality so that they can appear in all the Π groups.
- Add one additional variable to the j repeating variables and form a power product. Algebraically find the exponents which make the product dimensionless.

Last, write the final non-dimensional function, and check to make sure that all the Π groups are dimensionless.

5.2 Dimensional Analysis for the Coanda Jet

The various parameters considered for the study of the COANDA jet were:

Table 5.1: Parameters affecting the behavior of the air jet and their dimensions

Parameter	Symbol	Unit
Air Supply Gage Pressure	P	$ML^{-1}T^{-2}$
Radius of Curvature	R	L
Nozzle Width	b	L
Height Difference	h	L
Air Velocity	V	LT^{-1}
Density	ρ	ML^{-3}
Kinematic Viscosity	ν	L^2T^{-1}
Surface Roughness	ϵ	L

The primary dimensions are considered to be:

- (Mass) Density
- (Length) Radius of Curvature
- (Time) Velocity

We can see that there are three primary dimensions (mass, length & time) and the number of control dimensions is eight. Thus according to the Buckingham Pi Theorem, we can have no more than $8 - 3 = 5$ dimensionless numbers which can be used to predict the above flow.

To find out these non-dimensional numbers, we use the following technique (commonly known as the power technique).

We form a Π group such that

$$\pi = P^a R^b b^c h^d V^e \rho^f v^g \varepsilon^h$$

Thus we have,

$$\pi = (ML^{-1}T^{-2})^a (L)^b (L)^c (L)^d (LT^{-1})^e (ML^{-3})^f (L^2T^{-1})^g (L)^h$$

Now for the whole family, we have (comparing the powers on both the sides) :

$$M : a + f = 0 \quad (5.1)$$

$$L : -a + b + c + d + e - 3f + 2g + h = 0 \quad (5.2)$$

$$T : -2a - e - g = 0 \quad (5.3)$$

We have three equations and eight unknowns. Thus the matrix of the coefficients has three rows and eight columns and so the rank (the maximum order of the non-vanishing determinant) is three. Algebraic theory states that there will be a unique solution of the equations for any three terms whatever choice is made for the remaining terms other than all zeros. The number of terms equals the rank of the determinant. In most cases the rank equals the number of fundamental units. Now we shall solve for the values of b, f, e since the repeating parameters are chosen to be R, ρ , V.

Table 5.2: Matrix of coefficients for the Π group

	P	R	b	h	V	ρ	v	ε
M	a						f	
L	-a	b	c	d	e	-3f	2g	h
T	-2a				-e		-g	

Case 1: Using $a = 1$ and all others as $= 0$.

$$(5.1) \Rightarrow 1 + f = 0 \quad (5.4)$$

$$(5.2) \Rightarrow -1 + b + e - 3f = 0 \quad (5.5)$$

$$(5.3) \Rightarrow -2 - e - 0 = 0 \quad (5.6)$$

From eqn. (5.4) we get, $f = -1$

From eqn. (5.6) we get, $e = -2$

Substituting the above two results in the eqn. (5.5) we get, $b = 0$

Thus the non-dimensional number we get is $P^1 R^0 \nu^{-2} \rho^{-1}$ or $\frac{P}{\rho V^2}$ which is known

the Euler number.

Case 2: Using $c = 1$ and all others as $= 0$.

$$(5.1) \Rightarrow 0 + f = 0 \quad (5.7)$$

$$(5.2) \Rightarrow b + 1 + e - 3f = 0 \quad (5.8)$$

$$(5.3) \Rightarrow e = 0 \quad (5.9)$$

From eqn. (5.7) we get, $f = 0$

From eqn. (5.9) we get, $e = 0$

Substituting this in eqn. (5.8) we get, $b = -1$

Thus the non-dimensional no. becomes $b^{-1} R^{-1}$ or $\frac{b}{R}$ which is a geometry

parameter.

Case 3: Using $d = 1$ and all others as $= 0$.

$$(5.1) \Rightarrow 0 + f = 0 \quad (5.10)$$

$$(5.2) \Rightarrow b + 1 + e - 3f = 0 \quad (5.11)$$

$$(5.3) \Rightarrow -e = 0 \quad (5.12)$$

From eqn. (5.10) we get, $f = 0$

From eqn. (5.12) we get, $e = 0$

Substituting this in eqn. (5.11) we get, $b = -1$

Thus the non-dimensional number is $h^{-1}R^{-1}$ or $\frac{h}{R}$ which is another geometry number.

Case 4: Using $g = 1$ and all others as $= 0$.

$$(5.1) \Rightarrow f = 0 \quad (5.13)$$

$$(5.2) \Rightarrow b + e - 3f + 2 = 0 \quad (5.14)$$

$$(5.3) \Rightarrow -e - 1 = 0 \quad (5.15)$$

From eqn. (5.13) we get, $f = 0$

From eqn. (5.15) we get, $e = -1$

substituting this in eqn. (5.14) we get, $b = -1$

Thus the non-dimensional number is $R^{-1}V^{-1}\nu^1$ or $\frac{\nu}{RV}$ which is the inverse of the Reynolds number.

Case 5: Using $h = 1$ and all others as $= 0$

$$(5.1) \Rightarrow f = 0 \quad (5.16)$$

$$(5.2) \Rightarrow b + e - 3f + 1 = 0 \quad (5.17)$$

$$(5.3) \Rightarrow -e = 0 \quad (5.18)$$

From eqn. (5.16) we get, $f = 0$

From eqn. (5.18) we get, $e = 0$

Substituting this in eqn. (5.17) we get, $b = -1$

Thus the non-dimensional number is $\varepsilon^1 R^{-1}$ or $\frac{\varepsilon}{R}$ which is a surface roughness number.

Thus the non-dimensional numbers that we obtain by performing the power technique are:

Table 5.3: Non-dimensional numbers formed using the specified parameters

Reynolds number	$\frac{RV}{\nu}$
Euler number	$\frac{P}{\rho V^2}$
Surface roughness parameter	$\frac{\varepsilon}{R}$
Geometry parameter 1	$\frac{b}{R}$
Geometry parameter 2	$\frac{h}{R}$

CHAPTER 6

CONCLUSIONS

The following conclusions can be drawn from the present study:

- 1) The air jet as it exits out of the Coanda nozzle exhibits three distinct behavioral regions: the Separated jet region (where the jet separates from the solid surface), the Attached jet region (where the jet attaches to the solid surface) and the Bistable region (where the jet either behaves as a separated or attached jet). There exist basically two threshold values of supply air pressure: below the first value, the jet is completely in the separated region; above the second value, it is always attached to the surface; and, in the region between these two threshold values, the air jet will either be separated or attached depending upon the direction it was deflected earlier.
- 2) Upon analysis of the data for the second (upper) threshold values, we can see that the effect of the nozzle width and pressure is governed by the function given below:

$$\left(1 + 0.502 \frac{b}{R}\right) \ln\left(\frac{PR^2}{\rho v^2}\right)$$

- 3) The same kind of function could not be arrived at for predicting the behavior of the air jet with respect to the height of the nozzle block, but the graphs do show that there exists a value of h which gives the lowest value of critical threshold value of pressure, and this value seems to be a constant 0.1 inches irrespective of the values of the other parameters. For values of h below this

critical value (for example, $h = 0$ inches), the threshold pressure is very high, while for values above this (for example, $h = 0.2$ inches), the threshold starts to gradually increase again.

- 4) The effect of the radius of curvature of the convex surface on the behavior of the air jet is that as the radius is increased, the threshold pressure required for attachment of the jet decreases. This is in accordance with the theory that as the radius of curvature is smoothed, the tendency of the jet to attach is increased.
- 5) In the pressure profile existing between the rigid web and the nozzle block, there occurs entrainment of the surrounding air before the nozzle exit which agrees with previous research work done on this subject.
- 6) For the pressure profile existing between the air jet and the rigid web, it is noticed that as the supply pressure is increased, the peaks and the troughs in the profile become more pronounced.
- 7) It is also noticed that though the frictional force increases with increase in the supply air pressure, the rate of increase seems to decrease suggesting that there might be an upper value of supply pressure, beyond which any increase in the pressure would not give a significant enhancement in the frictional force exerted on the web.
- 8) The experimental results obtained as a result of this study seem to match quite consistently with data arrived at by computational methods through the work of Thirumal (1998).

CHAPTER 7

RECOMMENDATIONS FOR FUTURE STUDY

The following recommendations have been proposed to extend this work beyond the current accomplishments.

- 1) One of the main causes for uncertainty in the first series of experiments is the method used for judging the direction of travel of the air jet. This can be substantially reduced by using better flow visualization techniques (like tufts, etc.). Another method that could be used would be a traversing pitot tube which would also give an insight into the velocity profile of the air jet.
- 2) Another improvement to the existing design would be the use of an air compressor with a wider range of supply pressure. The controls of the air compressor can also be adjusted so as to minimize the fluctuations of the supply air pressure, since the data has to be recorded over a length of time for the second series of experiments.
- 3) The behavior of the Coanda air jet can be further studied computationally to arrive at the complete governing equation, this time including the effect of other parameters like the surface roughness of the nozzle, the geometry of the nozzle surface, etc. This will be of use in obtaining an optimal design for a Coanda nozzle.

- 4) The surface roughness of the rigid web in the second series of experiments can also be closely monitored so as to increase the accuracy of the aerodynamic friction forces measured.
- 5) The above study can be extended to webs that are both flexible and which are moving, to correspond to conditions in the industry.
- 6) In the industry, the web flutters when traveling around air-turn bars. This phenomenon might also occur when a high speed Coanda air jet is used for web support and transport. This needs to be studied to avoid noise and web damage.
- 7) The use of the Coanda air jet, for control of the web speed and position should be studied using an active control of the supply air pressure.
- 8) The behavior of two self-facing Coanda nozzles has not been studied till now by any researcher. This study can be taken up either experimentally or computationally to explore the possibility of support, transport and positioning of webs.

REFERENCES

- Aravamudhan, V. R., Moretti, P. M. and Chang, Y. B., "An Experimental Study of the Coanda Effect for 90° Turning of Subsonic Air Jets", to be presented at the 1998 ASME Fluids Engineering Division Summer Meeting, June, 1998, Washington, DC.
- Baker, W. E., Westine, P. S. and Dodge, F. T., *Similarity Methods in Engineering Dynamics: Theory & Practice of Scale Modeling*, Spartan Books, 1973.
- Bourque, C. and Newman, B. G., "Reattachment of a Two-Dimensional, Incompressible Jet to an Adjacent Flat Plate", *Aeronautical Quarterly*, Vol. 11, pp. 192-204, 1960.
- Cornelius, K. C. and Lucius, G. A., "Physics of a Coanda Jet Detachment at High-Pressure Ratio", *Journal of Aircraft*, Vol. 31, No 3, pp. 591-597, 1994.
- Doebelin, E. O., *Measurement Systems: Application and Design*, 4th Edition, McGraw-Hill International Editions, 1966.
- Felsing, G. W. and Moller, P. S., "Coanda Flow Over a Circular Cylinder With Injection Normal to the Surface", *AIAA Journal*, Vol. 7, No. 5, pp. 842-846, 1969.
- Glauert, M. B., "The Wall Jet", *Journal of Fluid Mechanics*, Vol. 1, pp. 625-643, 1956.
- Gregory-Smith, D. G. and Gilchrist, A. R., "The Compressible Coanda Wall Jet - An Experimental Study of Jet Structure and Breakaway", *International Journal of Heat and Fluid Flow*, Vol. 8, No. 2, pp. 156-164, 1987.
- Langhaar, H. L., *Dimensional Analysis and Theory of Models*, John Wiley & Sons Inc., 1951.
- Marwood, R. M., "An Experimental Investigation of the Coanda Effect", M.S. Thesis, Purdue University, 1948.
- Morrison, J. F. and Gregory-Smith, D. G., "Calculation of an Axisymmetric Turbulent Wall Jet Over a Surface of Convex Curvature", *International Journal of Heat and Fluid Flow*, Vol. 5, No. 3, pp. 139-148, 1984.
- Murai, K., Kawashima, Y., Nakanishi, S. and Taga, M., "Self-Oscillation Phenomena of Turbulent Jets in a Channel", *Canadian Journal of Chemical Engineering*, Vol. 67, pp. 906-911, 1989.

Newman, B. G., "The Deflection of Plane Jets by Adjacent Boundaries - The Coanda Effect", *Boundary Layer and Flow Control-It's Principles and Applications*, Pergammon Press, pp. 232-265, 1961.

Paik, J., Zhang, J., Weintraub, R., Sinclair, B. G. and Leipmann, D., "The Coanda Jet is Not an All or Nothing Phenomenon: Partial Adherence of Jets to Surfaces Changes Jet Size: An In-Vitro Study Using Color Doppler Mapping and Laser Fluorescence Dye Visualization", *Circulation*, Vol. 94, No. 8, Abstract #2933, pp. 1500, 1996.

Reba, I., "Applications of the Coanda Effect", *Scientific American*, Vol. 214, No. 6, pp. 84-92, 1966.

Rodman, L. C., Wood, N. J. and Roberts, L., "Experimental Investigation of Straight and Curved Annular Wall Jets", *AIAA Journal*, Vol. 27, No. 8, pp. 1059-1067, August 1989.

Richmond, M. C. and Patel, V. C., "Convex and Concave Surface Curvature Effects in Wall-Bounded Turbulent Flows", *AIAA Journal*, Vol. 29, No. 6, pp. 895-902, June 1991.

Sawada, K. and Asami, K., "Numerical Study on the Underexpanded Coanda Jet", *Journal of Aircraft*, Vol. 34, No. 5, pp. 641-647, 1997.

Squire, H. B., "Jet Flow and it's Effect on Aircraft", *Aircraft Engineering*, Vol. 22, March 1950.

○ Tanaka, T., Tanaka, E. and Inoue, Y., "A Study on the Deflection and Reattachment of an Axisymmetric Radial Wall Jet (Deflection of Main Jet Near Nozzle)", *JSME International Journal*, Vol. 30, No. 266, pp. 1243-1247, 1987.

Thirumal, S. P., "A Computational Study of the Coanda Effect and its Implementation in Air Turn Bars", M.S. Thesis, Oklahoma State University, 1998.

△Wetmore, A. C., "Evaluation of a Coanda Nozzle for Pneumatic Conveying", M.S. Thesis, Oklahoma State University, 1972.

White, F. M., *Viscous Fluid Flow*, 2nd Edition, McGraw-Hill International Editions, 1974.

Wille, R. and Fernholz, H., "Report on the First European Mechanics Colloquium on the Coanda Effect", *Journal of Fluid Mechanics*, Vol. 23, No. 4, pp. 801-819, 1965.

APPENDIX

Programming on LabVIEW for the Coanda Jet Experiment

The steps followed for programming on LabVIEW for the Coanda Jet experiment are described in this appendix. The program that was written for this particular application is shown in Figs. A.1 and A.2 respectively as the front and back panels. One important point to be remembered is that the programs written in LabVIEW are graphical and not text based.

One of the main points to be noted is that while the data is being sampled, the individual sampled readings might deviate from the mean values and so it is always a good practice to get a set of data and then find the average of these. To do this, we had to run the program using a loop mode so that a large set of the same data was obtained.

The outputs from the load cell and pressure transducer were connected to specific channels in the Analog to Digital Converter box that we used. These channels were specified in our program by using an inbuilt function called "AI Sample Channel vi": this enabled us to instruct the program to obtain the data from the specified channel of the Analog to Digital Converter box. In our program, the channels in the A/D converter box were specified according to the following Table A.1:

Table A.1: Connections given for the devices in the AD Converter

Channel Number	Device/Instrument
0	Pressure Transducer
1	Load Cell
3	Energy Supplied to the Load Cell

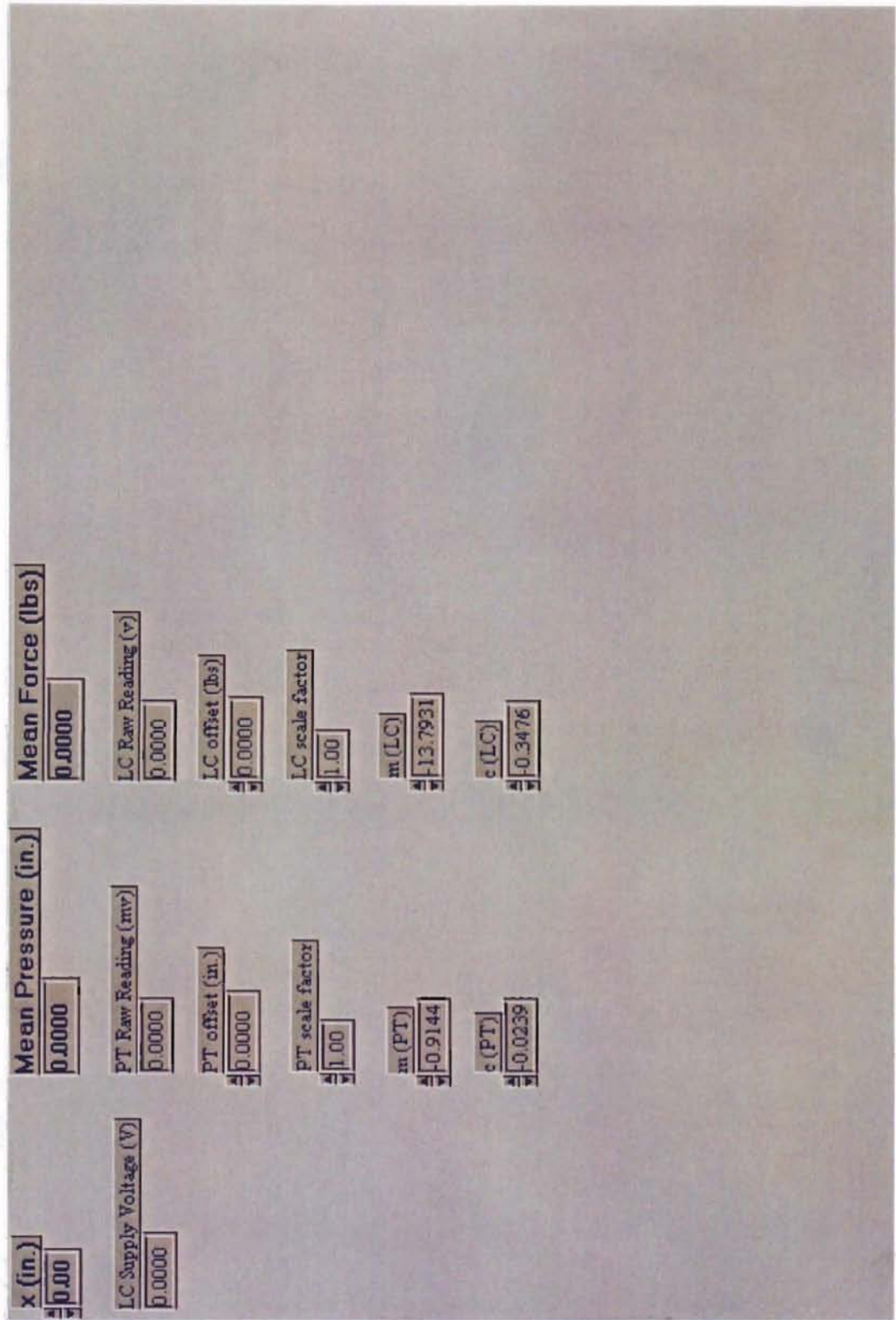


Figure A.1: The Front Panel of the program code for testing the Coanda effect on a rigid web

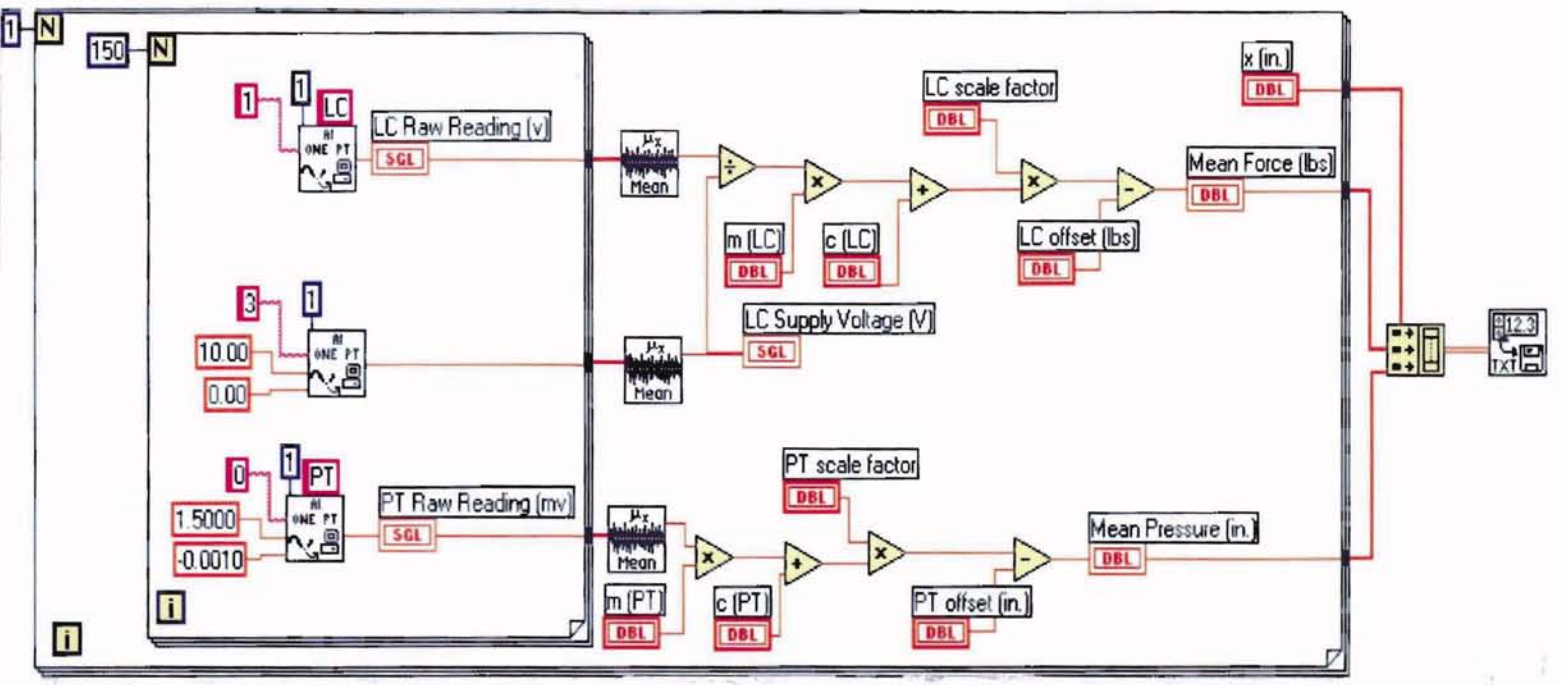


Figure A.2: The Diagram Window of the program code for testing the Coanda effect on a rigid web

For each of the series of data the general order of flow was almost the same as seen in Fig. A.2. The output from the sub-vi was connected to an indicator placed on the front panel so that we could view the data being acquired (in real time). The number of data to be collected for finding the mean was specified as the number of times that the loop has to be repeated and for this application, we specified this value to be 150. Outside the loop we made use of another inbuilt function (called "mean.vi") by which we can find the mean of the set of data collected. The output from this was also given to an indicator (again to view the data in real time). Using numerical manipulations, (like the adding, subtracting, multiplication, etc.), the raw data output from the AI sample channel vi was converted to the actual value. These manipulations were done according to the calibration curves that we obtained for the pressure transducer and the load cell. At the end of this stage, the data was in the actual value but still not in the required units. To convert the data into the required units, the same procedure (using the adding, etc. circuits) was followed and the data was converted into the actual values in the units required. All these manipulations and conversions were done using the numeric functions that are inbuilt into LabVIEW. Using the numeric operators, the output from this last indicator in the line was manipulated (according to the calibration curve) to get the output in the units desired. This same set of code was repeated for the load cell, the pressure

transducer and the power input to the load cell using appropriate values for the calibration curves.

Since the data had to be stored in text format, the output terminals of the final indicators were connected to an arraying function and then to a File I/O icon and this completed the program code used for the Coanda Jet experiment.

VITA

Vijay Raghavan Aravamudhan
Candidate for the Degree of
Master of Science

Thesis: AN EXPERIMENTAL STUDY OF THE COANDA AIR JET
AND ITS APPLICATION TO WEB SUPPORT AND TRACTION

Major Field: Mechanical Engineering

Biographical:

Personal Data: Born in Madras, India, on September 19, 1974, the son of S. Aravamudhan and K. Mythili.

Education: Received Bachelor of Engineering degree in Mechanical Engineering from University of Madras, India, in May 1996. Completed the requirements for Master of Science degree with a major in Mechanical Engineering at Oklahoma State University in May 1998.

Experience: Shop Floor Supervisor, Veekay Rubber Products, India, from May 1995-July 1996. Research Assistant in Web Handling Research Center from August 1996-present and Teaching Assistant in Mechanical and Aerospace Engineering Department, Oklahoma State University from January 1998-present.

Professional Memberships: Tau Beta Pi, American Society of Mechanical Engineers, Society of Mechanical Engineers (student Chapter, India)